Spring 2013

Jet-Cooled Spectroscopic Characterization of Anethole (methoxy-4-(prop-1-enyl)benzene), a Natual Styrene Derivative

Victoria P. Barber , '13

Jet-Cooled Spectroscopic Characterization of Anethole (methoxy-4-(prop-1-enyl)benzene), a Natural Styrene Derivative

Presented as a Senior Thesis by

Victoria Barber

Advisor: Josh J. Newby

Swarthmore College, Department of Chemistry and Biochemistry

May 2013

Table of Contents

Acknowledgements

I would first like to thank Josh Newby, for his help throughout my research. He has been instrumental in my work, and none of this would have happened without his guidance and support. I would also like to thank him for going out to Purdue University over winter break and acquiring the SVLF spectra, since most of this analysis would have been impossible without this data. I am grateful to Kathleen Howard and Paul Rablen for agreeing to serve on my committee. Thomas Stephenson has also been gracious enough to let us use his lab and equipment this year. Timothy Zwier at Purdue University allowed Dr. Newby to come out and use his lab to take some of our data. The computational resources of GridChem have been incredibly helpful in completing the large calculations this work entailed. None of this would have been possible without the financial support of Swarthmore College. I'd also like to acknowledge Maddy Amodio for her work this past summer and for collecting some of our first origin band SVLFs with me. Special thanks to Vienna Tran, Travis Mattingly, and Liz Williams for living in the seminar room with me during thesis crunch time, and making the writing process a bit more bearable. Thanks also to Andrew Waks, my favorite non-chemist thesis writing buddy who has been in the department keeping me company every night. Finally, I thank my fellow chemists of the Class of 2013, who have been my thesis writing buddies, and a wonderful support system throughout this year and the ones before.

Abstract

The molecular structure of anethole (methoxy-4-(prop-1-enyl)benzene), was investigated using Jet-Cooled UV spectroscopy. A laser-induced fluorescence spectrum was obtained of the S_1-S_0 transition. Two 0^0_0 transitions were observed in the LIF spectrum, separated by 69 cm^{-1}, and were assigned to the *syn* and *anti* conformers of anethole. Single vibronic level fluorescence spectra were obtained for both of the origin transitions. Bands of the SVLF spectrum of each conformer were assigned by comparison with theoretical calculations at the DFT/B3LYP, 6-311G++(d,p) level of theory, as well as experimental information from similar molecules. In order to assign the LIF spectrum further, SVLF spectra were obtained of many of the LIF transitions, and assigned where possible. SVLF transitions of particular importance are the 63^0_2 and the 39^0_1, which appear reliably in almost all SVLF spectra, but at slightly different frequencies for each conformer, allowing the assignment of SVLF spectra to a specific conformation of anethole. LIF and SVLF data indicated the possibility of water-anethole van der Waals clusters, which were confirmed by adding water to the jet. Additionally, we performed potential energy scans of the vinyl and methoxy rotations of anethole, and fit these scans in order to determine parameters for anharmonicity and the barrier to rotation. By comparing to experimental fits in the literature, we determined that MP2 calculations predicted the barrier to rotation best, but HF calculations did a better job of predicting the anharmonicity. Opportunities for future work include the modeling of the potential using experimental data, further investigation of anethole-water clusters, finishing the assignment of the LIF and SVLF, and possibly investigating the spectroscopy of *cis*-anethole.

Introduction

This work undertakes a jet-cooled spectroscopic study of the ground (S_0) and first excited (S_1) electronic states of *trans*-Anethole ((*E*)-1-methoxy-4-(1-propenyl)benzene) (see Figure 1). *trans*-Anethole, the only naturally occuring isomer of anethole, is an essential oil commonly found in anise and fennel. It is found naturally in at least 20 food products, as well as being used as a flavoring agent, and can be extracted from natural sources or synthesized. It is estimated that 0.75 million metric tons of anethole are released into the atmosphere by natural sources each year[2]. While this is not a particularly large amount in comparison with the total mass of the atmosphere, it does indicate that Anethole is present in at least some amount in the environment, and is constantly interacting with UV and visible light. It is therefore a potential participant in atmospheric gas phase reactions. In fact, *trans*-anethole may dimerize or isomerize to *cis*-anethole due to exposure to UV and visible light.[3] Photochemical reactions of anethole with other organic molecules, including also been observed,[4] suggesting anethole is reactions, and making its interaction with UV and visible light a rich subject for further study.

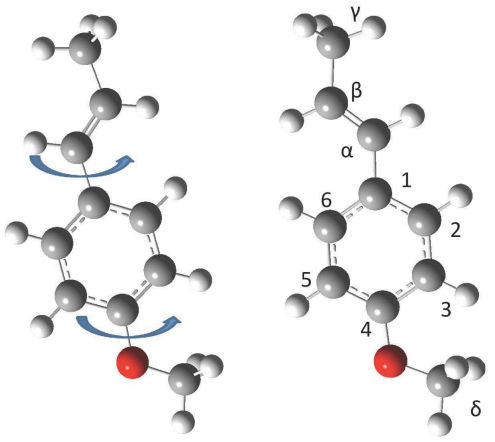

Figure 1. The DFT-B3LYP 6-311g++(d,p) optimized structure of syn (left) and anti (right) conformers of anethole. Carbons are labeled for clarity and are referred to by these labels throughout this work. Motions of particular interest are shown with arrows.

Anethole is also styrene derivative. Styrene is a well characterized molecule, and its derivatives play an important role in

many aspects of organic chemistry. It is important in the understanding of conjugation and aromaticity, it is a useful synthetic intermediate, particularly in the formation of polymers, and it is a substructure of many natural products, not only anethole[5]. Anethole is a particularly interesting styrene derivative because it is "floppy." It has several different possible coordinates of motion. There are two potential methyl rotors. Additionally, both the vinyl group and the methoxy group should be able to rotate freely, so long as they have the energy necessary to overcome the barrier to this rotation, which, since the rotation is around a single bond, would be expected to be quite small.

The goal of this work was to gain a better idea of what *trans*-anethole looks like at the molecular level, and to examine its vibrational modes and molecular motions in both the ground and first excited electronic states. We were also interested in studying the isomerization between the two conformers. Additionally, we sought to compare anethole to other molecules of similar structures. We use a combination of spectroscopy and *ab initio* calculations to investigate these goals.

Jet-Cooling: A Brief Introduction

The jet-cooling technique is essential to our method, as it allowed us to take the vibrationally resolved, electronic spectrum of a relatively large molecule. We are interested in the properties of the gas phase, isolated molecule. Yet, if the molecule is heated to produce a higher vapor pressure, more, higher energy states of the molecule become populated, and the spectrum becomes so thermally congested that very little vibrational information is visible. Assuming anethole follows the Boltzmann

distribution, by cooling the sample we can greatly decrease the number of levels that have any appreciable population. However, if the molecule is cooled by the use of a refrigerant, the effects of intermolecular interactions will dominate the spectra, and very little information about isolated molecules will be available[6]. Jet cooling provides an elegant solution: anethole, entrained in helium, is expanded through a pin-hole into a vacuum. During the expansion, the internal degrees of freedom of the molecule are cooled by collisions with the carrier gas, bringing almost all of the molecules to their zero-point level, yet keeping them at low enough densities to be essentially isolated[6,7,8]. When the gas jet is overlapped with a laser, the result is a spectrum that minimizes both intermolecular effects and "hot bands"- transitions that begin at a higher level than the ground state. This makes the spectra collected significantly simpler, and allows the resolution of individual peaks that correspond to specific vibrational states.

Laser Induced Fluorescence and Single Vibronic Level Fluorescence Spectroscopy

Two different types of jet-cooled spectroscopy, laser induced fluorescence (LIF) and single vibronic level fluorescence (SVLF) are used in this work. For solution phase spectroscopy, we would normally collect an absorption spectrum, but in the gas phase, the sample is so diffuse that absorption spectroscopy would have a very poor sensitivity and signal to noise ratio. Instead, absorption must be measured indirectly[7,8]. An LIF spectrum (sometimes referred to as a fluorescence excitation or FE spectrum), however, provides similar information about the frequencies at which an excitation occurs. The laser is scanned through a range of wavelengths. When the frequency of the laser

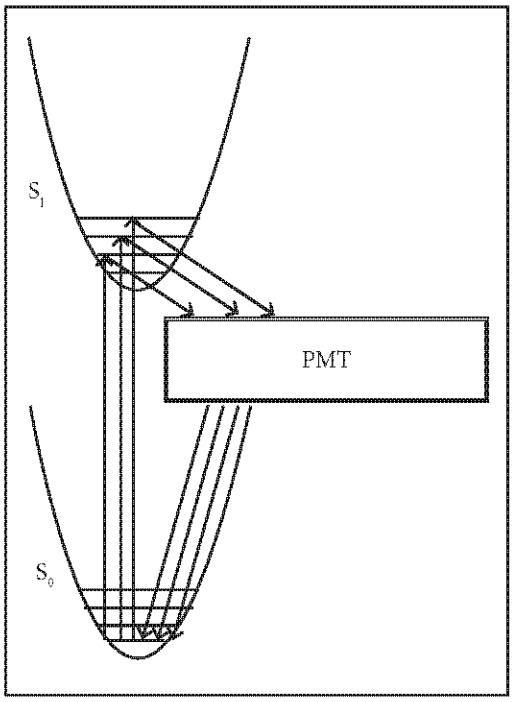

Figure 2. A schematic representation of LIF spectroscopy. The laser is scanned through a range of wavelengths, exciting a variety of vibrational transitions. The resulting fluorescence is measured using a photomultiplier tube. This technique gives information about the excited electronic state

resonates with the energy needed to produce a transition from the zero-point level of the ground electronic state to some vibrational level in the excited electronic state, the molecule will absorb photons, and then fluoresce. The resulting fluorescence intensity is measured, in our case via a photomultiplier tube. This spectrum is essentially the product of the absorption spectrum and the fluorescence quantum yield. Therefore, for quantum efficiencies near one, the LIF spectrum is simply a more sensitive way of measuring an absorption spectrum[6]. If the molecules are at the zero-point level of the ground electronic state before excitation, than the LIF spectrum gives information about the frequencies of the vibrational modes in the excited state (see Figure 2).

In SVLF spectroscopy (also sometimes referred to as dispersed fluorescence or DF spectroscopy), the excitation laser is fixed on a particular wavelength where an absorption is known to occur (the LIF spectrum becomes a useful tool in this case because it lets us know at what frequencies absorbance and subsequent fluorescence will happen). The molecule then emits the light, and relaxes to a variety of vibrational levels in the excited state. The fluorescence is dispersed with a monochromator, and both the intensity and the wavelength are measured, in our case using a charge coupled device

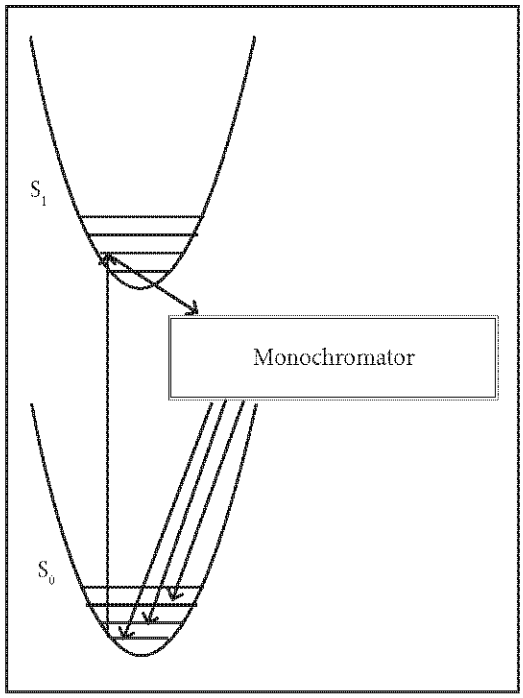

Figure 3. A schematic representation of SVLF spectroscopy. The laser is set to the frequency of a known transition, and the resulting fluorescence is measured with a monochromator and CCD, which allows the measurement of both the intensity and the wavelength. This technique gives information about the ground electronic state vibrational frequencies.

(CCD). The pattern of this fluorescence is highly dependent on the state to which the molecule was excited, and gives information about the frequencies of vibrations in the ground state (see Figure 3). As the molecule falls back to the ground electronic state, it will not necessarily fall directly to the ground vibrational level. Therefore fluoresced photons will often be of a lower frequency that the excitation. The differences between the excitation energy and the energies of the fluoresced photons corresponds to the frequencies of vibrations in the ground electronic state.

Previous Studies of Anethole

Previous work suggests that anethole has two conformations, a *syn* and an *anti* rotamer, separated by an energy barrier that would likely be negligible at room temperature. Under these conditions, anethole would change freely between its two forms. However, in a jet-cooled environment, the molecule does not have the necessary energy to overcome the barrier and thus gets locked into one configuration. Grassian *et al.*[5] have previously studied the electronic excitation spectrum of jet cooled, gas phase, anethole and observed two intense transitions, at 32889 and 32958 cm^{-1}, and assigned them tentatively to the origin bands (the transitions from the zero point level in the S_0

state to the zero point level in the S_1 state) of the *syn* and *anti* conformers, respectively, based on the intensities of the bands, and their locations at the lowest energy end of the spectrum. Additionally, the energies of these transitions are comparable to the origin bands of 3-methylstyrene and m-cresol . This same work suggests that this observation, along with several other studies of similar styrene derivatives, as reasonable proof that the vinyl group of anethole is planar. It did not, however, undertake a complete characterization of the two conformers and their vibrational modes

Literature study of (E)-Paravinylacetylene

More complete studies, however, do exist on several molecules similar to anethole. Much of our work is based on techniques used by Liu *et al.* in studying (E)-phenylvinylacetylene (PVA)[9]. These isomers are close structural analogues of styrene, like anethole, and exhibit a π-π^* transition for the S_0-S_1 transition. This study undertook jet-cooled LIF and SVLF spectroscopy of the two isomers under very similar conditions to ours (in fact, most of the SVLF spectra presented in this work were taken in using this same experimental set-up at Purdue University).

Liu *et al.*[9] found 48 calculated normal modes of (E)-PVA, 33 in plane with a' symmetry, and 15 out of plane with a" symmetry using the density functional theory with the Berny3LYP functional[10,11] and the 6-311++g(d,p)[12-13] basis set. By electric dipole selection rules, all a' modes are allowed, while only combination bands or overtones of a" transitions are allowed[14]. The DFT calculations were used to assist in assigning the SVLF spectra, and reliably calculated frequencies within less than 20 cm^{-1} of the experimentally observed frequency, and in many cases less than 10 cm^{-1}. In the LIF

spectrum, the most intense transitions, that is, those with the most Franck-Condon activity, are those involving the ring. These modes include the 1, 6, 12, and 13 benzene like modes (in the Wilson numbering scheme[15]). By taking SVLF spectra of many of the observed bands in the LIF, they were able to assign most transitions. For in-plane vibrations, this proved to be quite simple, as these SVLF spectra tend to exhibit a false origin that corresponds to the transition from 1quanta in the excited state of a vibration to one quanta in the ground state. Furthermore, these spectra tend to be relatively simple.

However, this study notes that styrene derivatives (and this molecule in particular, due to its longer conjugated side chain) exhibit an effect in which the physical form of the normal modes change from one electronic state to another, known as Duschinsky mixing[16]. This complicates the assignment of the LIF spectrum quite a bit, especially since excited state configuration interaction singlet (CIS)[17] calculations were found not to be reliable enough to be helpful in making assignments. Furthermore, the modes that exhibited mixing also tended to be a" vibrations, meaning that only overtones of these vibrations were allowed. In order to assign these mixed modes, the identification and assignment of hot bands (bands originating from an energy level other than the zero-point) proved to be useful. These bands carry information about frequency differences between modes in the S_0 and the S_1 state, since they can arise from the same vibration in the ground state, rather than from the zero point level.

This study was particularly concerned with the vinyl torsion, both because a progression of overtones of this vibrational mode can be observed in the SVLF spectra, and because, in the excited state, the π-π^* transition changes the bond order of the bond from the vinyl group to the ring in styrene. The large change in the vinyl torsional mode

frequency (from 43 cm^{-1} in the ground state to 348 cm^{-1} in the excited state) can be attributed to this change. This work was able to fit the observed overtone progression to a truncated Fourier series[9, 18]:

$$V(\varphi) = \frac{1}{2}\sum_{n=1}^{4} V_n[1 - \cos(n\varphi)] \quad (1)$$

where the V_2 term corresponds to the barrier height, and the V_4 term is related to anharmonicity. The other terms are expected to be insignificant. They found a V_2 of 688 cm^{-1} and a V_4 of -114. The large, negative value of the V_4 term indicates a flat bottomed potential. Styrene also exhibits this behavior, with a V_4 term of -275 cm^{-1}.[19] While conjugation effects favor a planar conformation, steric considerations, as well as hyperconjugation, favor nonplanarity. The conjugation effect is dominant, but only marginally, which leads to the large anharmonicity of the potential[18]. This study also compared this simulated potential based on experimental data to one calculated from *ab initio* calculations. They found that while DFT calculations yielded the same overall shape of the potential, and Moller-Plesset second order (MP2)[20-21] calculations did not, MP2 calculation barrier to the rotation much closer than any others (though it still overestimated by 158 cm^{-1}. However, the MP2 calculations do not come as close to predicting the V_4 term, most likely because it fails to account for the planar geometry of the molecule[9]. In fact, all calculations significantly overestimated the magnitude of the V_4 term, though Hartree Fock (HF)[22-23] comes the closest. Interestingly, for styrene, while DFT/B3LYP calculations significantly overestimate the barrier to rotation, they come very close in predicting the V_4 term, (-275 cm^{-1} for the experimental simulation vs. -274 cm^{-1} for the *ab initio* calculation).

Literature Study of trans-β-methylstyrene

Sinclair *et al.* obtained jet cooled SVLF and fluorescence excitation spectra of *trans*-β-Therefore, methylstyrene (*t*βms), a molecule even more similar to anethole than (E)-PVA and another styrene derivatives[18]. Many bands in both the SVLF spectrum and the LIF spectrum were assigned in this work, which made it an invaluable tool in assigning anethole spectra. They calculated 42 normal vibration modes of this molecule, and an additional five modes corresponding to the vibrations of the methyl group. They did not include these internal methyl vibrations in their analysis, and for this reason the numbering scheme used in this work differs slightly from the Mulliken scheme[1]. They observed that the majority of the fluorescence excitation spectrum was dominated by bands due to benzene type modes, but were additionally able to assign transitions involving the ν_{42} vinyl torsion and the ν_{41} vinyl out of plane bend (numbered according to the Mulliken scheme[1]), including the 42_0^2 at $0^0_0 + 329$ cm^{-1} and the 41_0^2 at $0^0_0 + 242$ cm^{-1}, where 0^0_0 is the origin peak at 34760 cm^{-1}.[18] Notably, the frequency of the ν_{42} vibrations in the excited state is significantly higher than in the ground state, where it appears at $0^0_0 + 67$ cm^{-1}. A similar change in frequency is also observed in styrene, from $0^0_0 + 86$ cm^{-1} in the ground state to $0^0_0 + 371$ cm^{-1}. The increase in the ν_{42} frequency in the excited state corresponds to a much higher to the vinyl rotation in the excited state than in the ground, and is likely due to an increased π-bonding character in the excited state.

In styrene, it was observed that there is a very strong Duschinksky mixing effect, in which the ν_{42} and ν_{41} modes are much more mixed in the excited state as opposed to

the ground. In the spectroscopy, this manifests itself as transitions such as $41^1_0 42^0_n$ where n is odd, which allows access to vibrational levels in S_0 that involve odd quanta of ν_{42}.[24] This same Duschinsky effect was observed in the *t*βms LIF spectrum, suggesting that these modes are mixed in the excited state. This effect also causes additional congestion in the LIF spectrum[18].

Sinclair *et al.* observed a progression of the even quanta of the ν_{42} up to 6 quanta, as well as odd levels of ν_{42} up to 5 quanta from combination bands, and from this data were also able to model the torsional potential in the ground state, according to the truncated Fourier series in equation 1. In *t*βms, the V_2 term of this fit is 855 cm^{-1} and the V_4 term is -218 cm^{-1}, a large negative number that indicates the potential is flat bottomed, as in (E)-PVA and styrene[19]. Sinclair *et al.* were not able to model the S_1 torsional potential, because a progression of the ν_{42} was not observed or assigned in the excitation spectra.

They were also interested in the methyl torsional mode, but very little activity of the methyl torsional mode was observed in the SVLF spectrum, and none was visible in the LIF. A very weak band was observed 217 cm^{-1} below the excitation energy in the origin SVLF, and was attributed to a the methyl torsion fundamental in combination with ν_{42}. This assignment was based mainly on the process of elimination and therefore was somewhat tentative. However, they were able to use this single frequency to estimate the barrier height of the torsion. Unlike the vinyl torsion, the methyl torsion should exhibit a 3-fold barrier. The calculated value for the barrier height was 675 cm^{-1}, a value similar to the propene methyl torsional barrier of 693 cm^{-1},[25] which they took as a confirmation of their assignment. The close proximity to the value for styrene suggests that the phenyl

group has very little effect on the methyl torsional barrier. This group concluded that the methyl torsion is essentially unaffected by electronic excitation, a difficult conclusion to accept given that the effect of the excitation would be expected to extend through the double bond of the vinyl group to the β carbon. There is some conflict as to whether this is in agreement with previous studies, as methyl torsions are only seen in some styrene derivatives[18].

Literature Study of Anisole

A similar study also exists on anisole,[26] which is not considered a styrene derivative. This work analyzed the S_1-S_0 transition of anisole by LIF and SVLF spectroscopy in a supersonic jet, aided by *ab initio* calculations. Additionally, the same studies were performed on d_3-anisole, with the goal of understanding the contribution of the methoxy group to the vibrational structure.

The origin band for anisole in the LIF spectrum was observed at 33384 cm^{-1}, and for d_3-anisole at 36387 cm^{-1}. Such a small shift indicates little change in the electronic structure due to the methyl dueteration, at least in the S_0 and S_1 states. It was also concluded that the dueteration did not affect molecular symmetry, and overall the LIF spectra look quite similar, with shifts in frequencies but similarities with regards to the intensity, resolution, and number of peaks. One more major difference is in the region around 900 cm^{-1} above the origins. In the spectrum for anisole, these peaks are barely resolved, but in d_3-anisole there are 3 distinct peaks. They theorize that this is due either

to frequency shifts which move these bands further apart, or possibly to a decrease in vibrational mixing of these levels.

As with the LIF spectra, the SVLF spectra of the origin bands are very similar, but with several differences in band positions, particularly the methoxy bending motion which appears at 257 cm^{-1} below the excitation wavelength for anisole, and 232 cm^{-1} below the excitation wavelength for d_3-anisole, suggesting that the more massive methoxy group leads to a decreased frequency of the vibration. Interestingly, and unlike in styrene derivatives, in which a pure vinyl torsional vibration is visible in most spectra, no pure methoxy torsion was visible in either SVLF origin spectrum. We only observe the methoxy torsion in the LIF spectrum, and only in concert with other vibrations. Unlike the spectrum of *trans*-β-methylstyrene, the DF and LIF spectra of anisole are dominated by transitions that are almost equally spaced. These modes are assigned as overtones and combinations of two vibrational modes, the 10b and 16a benzene-like modes (according to the Wilson numbering scheme[15]).

Literature Study of 4-methoxystyrene

A separate study by Ribeiro-Claro *et al.*[27] focused on the jet-cooled spectroscopy of 4-methoxystyrene (4MEOSTY). Similarly to anethole, 4MEOSTY is presumed to have a planar heavy atom configuration, and thus have 2 rotamers, a *syn* and an *anti* conformation. They obtained the FE and SVLF spectra of 4MEOSTY, and used *ab initio* calculations along with Raman and IR spectra to make vibrational assignments where possible.

They observed 2 origin peaks in the FE spectrum at 33248.3 cm^{-1} 33324.7 cm^{-1}. These bands were identified as origins because they did not belong to any progression, and appeared at the lowest frequency in the spectrum. Based on the planarity of 4MEOSTY, these two origins were assumed to belong to two different rotamers, a *syn* and *anti* conformation.

The only SVLF spectra presented in this paper are those of these two origin bands. These two SVLF spectra are, in many respects, quite similar, and contain some bands of very similar intensities and frequencies about the excitation frequency. However, there are also obvious differences. For example, there is a band 80.2 cm^{-1} from the excitation frequency in one spectrum that is quite intense. In the second spectrum, this band is replaced by a much weaker band separated by 85.6 cm^{-1} from the excitation frequency. This suggests that these two spectra are of a very similar transition in slightly different molecules, consistent with the theory of two rotamers. While they assigned this low frequency band to 2 quanta of the vinyl torsional vibration, only a few other bands of the SVLF spectrum were assigned.

They did, however, assign many of the vibrations in both the Raman (in both the solid and liquid phase) and FTIR spectroscopy (in the liquid phase). Unfortunately, unlike SVLF spectroscopy, these spectra do not allow for the separation of the two rotamers, so small differences in the frequencies of vibrations cannot be observed, and for many of these vibrations only one frequency is listed for both conformers, unless the frequencies of the two conformers are different enough to be resolved. Furthermore, these techniques can only provide information about the ground state of the molecule, as the incident radiation used is not enough to excite an electronic transition. They therefore

provide little help in analyzing the FE spectrum. They were, however able to use the Raman data to assign the origin bands to a more and less stable conformer, though they did not definitively assign these conformers to absolute configurations. The more stable isomer was determined to be the one with its origin at a higher frequency, and was tentatively assigned to the anti conformer[27].

Ribeiro-Claro *et al.* additionally modeled the vinyl torsional potential. However, unlike Sinclair *et al.*, they had only two pieces of data on which to base the parameters of the Fourier transform (see equation 1): the frequencies of the 2 quanta of the torsional frequencies for both conformers. Additionally, there is the added complication that the V_2 and V_4 parameters of the fit must be supplemented by an additional odd V term to account for the energy difference between the two conformers. There fitting process was therefore a bit different, and rather than calculating V_2, they set it at a "reasonable value" of 950 cm^{-1} (a value chosen based on previous work on 4-methylstyrene[28] and 4-fluorostyrene[29]). From this assumption, they were able to produce 2 possible sets of values of V_1 and V_4 that accurately reproduced the experimental data. Both fits had the value of v_4 equal to -210 cm^{-1} again a fairly large negative value similar in magnitude to the same parameter for styrene and *trans*-β-methylstyrene. The two fits differ in their values of V_1, the coefficient that corresponds to the energy difference of the 2 conformers. One fit fount this value to be 24 cm^{-1}, the other -174 cm^{-1}. Since $\varphi=0°$ was assigned to the *syn* rotamer, the positive value corresponds to the *syn* rotamer being more stable, while the negative value corresponded to the *anti* rotamer being more stable. Based on *ab initio* calculations, as well as the intensities of the two bands in the FE

spectrum, they were able to tentatively assign the *anti* conformer as the more stable configuration.

Investigation of Water-Anethole van der Waals Clusters

The analysis of anethole is further complicated by its potential to form van der Waals clusters. These aggregates form during the very first moments of the expansion, but then last relatively long, because the collision rates decrease in the vacuum. If these complexes represent a potential energy minimum, they will survive until some perturbation (such as the introduction of photons, or another collision) disturbs them[30]. Liu *et al.*[9] observed PVA-He Van der Waals complexes in the spectrum of PVA when the pressure of the helium carrier gas was decreased to 5.5 bar. These complexes, however, did disappear when He pressures were lowered.

Furthermore, anisole and other substituted benzenes have been shown to form van der Waals clusters with water. Becucci *et al.*[30] used molecular beam-electronic spectroscopy to study the anisole water complex intentionally, in combination with theoretical calculations. Using *ab initio* calculations, several possible conformations of the anisole water complex were identified, including several in which water acts as a hydrogen-donor, interacting with the lone pair on the oxygen atom, several in which water acts as the hydrogen-acceptor, with the water oxygen interacting with the methyl hydrogens, and two structures in which the π-cloud of the phenyl ring acts as the hydrogen accepter and the water as the hydrogen donor. According to calculations, the π-cloud interactions are expected to be most stable, with the most negative binding energy and lowest potential energy, while the structures with the water acting as the hydrogen

acceptor are expected to be the least stable. Interactions with the cloud were also calculated to have the highest percent population of minima. They observed, via resonance enhanced multiphoton ionization spectroscopy (REMPI), two origin bands at 36492 cm^{-1} and 36503 cm^{-1}, which they assigned to the anisole-water 1:2 and 1:1 complexes, respectively. The band corresponding to the 1:1 complex exhibits a blue shift from the origin band of isolated anethole of 119 cm^{-1}. By completing a high resolution spectrum of this band, they were able to determine that it corresponds to the arrangements in which water acts as a hydrogen donor[30].

Studies on other substituted benzenes, have also revealed that water can interact with the ring π system. Zwier *et al.* have published several studies on the microsolvation of benzene in water and methanol, and have seen structures of clusters including up to 8 solvent molecules[31,32,33]. These clusters form via a combination of hydrogen bonds between the solvent molecules, and bonds between the aromatic π-system and free OH groups of water. In fact, Barth *et al.*[34] note that anisole is the exception to the rule. This study looked at the OH vibrations of the water in the hydrogen bonded vs. the free water, and showed that the frequency shift caused by the hydrogen bond in anisole was much greater than that for other substituted benzenes, but more similar to the H_2O dimer stretch for the hydrogen donating molecule, suggesting that anisole, the hydrogen bonding is more similar to canonical hydrogen bonding, while in other substituted benzenes, the water is interacting by different means with the molecule. The most logical explanation for this observation is the interaction with the π system of the ring.

These works have been very useful in the analysis of the spectroscopy of anethole. Firstly, they validate the jet-cooling method for molecules similar to anethole,

and verify that theoretical calculations in the ground state provide a good starting point for peak assignments in the SVLF (though at computationally feasible levels of theory, excited state calculations prove to be of little help). Additionally, these previous studies provided useful standards to which anethole could be compared. *t*βms and 4MEOSTY in particular seems to have very similar spectra to anethole. Additionally, because the spectral features of anisole are so different from either *t*βms or 4MEOSTY, a particular interest in seeing how these two spectra would combine was developed. These previous studies also gave some idea of what to expect for anethole, including a flat bottomed potential for the vinyl rotation, a torsional mode with a much higher frequency in the excited than the ground state, and significant Duschinsky mixing in the excited state. Furthermore, since we did not take any special steps to exclude water from our jet, these studies alerted us to the possibility of anethole-water van der Waals complexes, a possibility that likely would have otherwise been ignored, since anethole is only slightly soluble in water in the liquid state[35].

Methods

All of the anethole used for this work was obtained from Eastman-Kodak and used without further purification. A gas chromatography/mass spectrometry (GC/MS) study was taken in order to determine the purity of anethole, and to ensure that none of the cis isomer was present. The results are shown in Figure 4. Small peaks are likely due to column contamination in the GC, which have been seen consistently with this equipment, while the largest peak at 25.811 min is due to *trans*-anethole, based on the MS results.

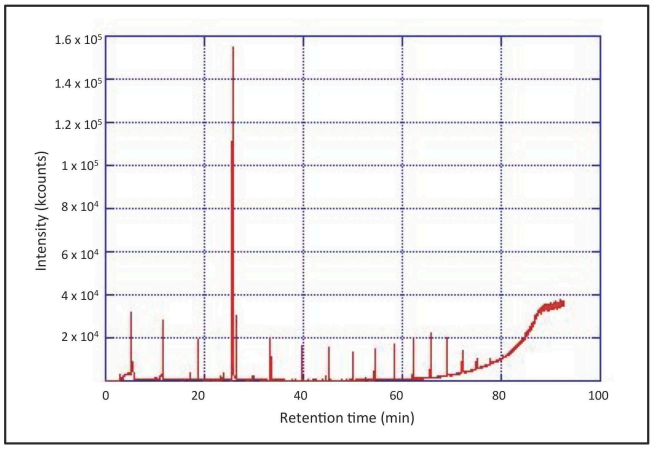

Figure 5. GC/MS purity check of our anethole sample. Unfortunately, not too much information can be gained from this, since the column has been contaminated. The large peak at 25.811 is anethole, while the other peaks are likely due to column bleeding.

Spectra were taken in two different labs: one at Swarthmore College and the other at Purdue University, with different experimental set-ups. All spectra are taken in a jet-cooled environment, in order to produce isolated molecules in the zero-point level. Briefly, a gas phase sample is entrained in a buffer gas, which is forced through a pin-hole into a high vacuum. The expansion of the sample molecule in to vacuum chamber is accompanied with many collisions with the buffer gas. These collisions transfer energy from the sample to the buffer gas, effectively cooling the sample. Jet-cooled methods often prepare molecules with translational temperatures of less than 1K[6]. This low temperature greatly simplifies the spectra since it allows the assumption in analysis that the molecules start from the ground state.

Two different types of spectroscopy were performed: laser induced fluorescence (LIF) and single vibronic level fluorescence (SVLF). In both experiments, a laser is used to excite the molecules of anethole and then their fluorescence after this excitation is measured. In LIF spectroscopy, the laser is scanned across a range of wavelengths that correspond to the wavelengths necessary to excite a molecule to its first electronic excited state (S_1). Depending on the wavelength of the laser, different vibronic levels within the two electronic states in question are accessed. We monitor the wavelength at which the laser is placed when fluorescence occurs, with the goal of determining what frequencies the molecule is absorbing. In this way, we can learn about the transitions to the excited state vibrations. A schematic of this experiment is shown in Figure 2. In SVLF experiments, the laser is trained on a specific transition observed in the LIF experiment, corresponding to excitation to a specific vibronic level. In this case, we measure the wavelengths and intensities of the emitted radiation. This technique is therefore useful for learning about the frequencies of vibrations in the ground electronic state (S_0). A schematic of this experiment is shown in Figure 3.

For all Swarthmore spectra, a nitrogen laser (Laser Photonics, UV24) was used to pump a tunable dye laser (Laser Photonics, DL-14P). For the LIF spectra, a dye change was necessary in order to cover the full range of the spectrum. Therefore, LIF spectra were obtained in two overlapping parts, with the intensities of the overlapping peaks matched for continuity. For the lower frequency region, Rhodamine 610 perchlorate (Exciton) was used in methanol. For the high frequency region, we used Rhodamine 590 chloride (Exciton) also in methanol. The dye laser output was frequency-doubled using an InRad Autotracker II. The visible output was separated from the UV by means of a

UG5, visible absorption filter. The UV laser light was then channeled through a chamber mounted directly above a diffusion pump (CVC, BVP-100) backed by a rotary-vane roughing pump (Welch Duo-Seal Vacuum pump, 1397). The laser beam was spatially and temporally overlapped with a gas-phase molecular jet of anethole.

To generate the molecular jet of anethole, a liquid sample of anethole was heated to approximately 80°C, by wrapping a reservoir chamber with heating rope, powered by a variac. The rough control provided by this setup meant that it was difficult to maintain a completely constant temperature between scans, and even across single scans, but temperature was maintained between roughly 75 and 80 °C for all acquisitions. Helium gas was then pumped through the reservoir in which the liquid was heated at a backing pressure of approximately 30 psi (unless otherwise specified). A pulsed valve, (General Valve, Series 9, 150 micron orifice) was used to deliver the sample to the chamber.

Laser Calibration

Calibrating our dye laser presented some problems. A mercury discharge lamp was used to calibrate, along with a monochromator (Spex industries, 500M) and charged-coupled device detector (Princeton Instruments, LM/CCD-2500-PB/UVAR), and the output was read on a personal computer using WinSpec/32 software (version 2.5.21.0). The hope was to calibrate the laser using the known wavelengths of the mercury emission. However, following this calibration it was determined that the measured origin band wavelengths were 1.44 nm below the origin bands measured by Grassian et. al.[5] There are several possible explanations for this, but most likely is that apparent laser wavelength shifts quite frequently, as we have observed throughout our experiments. It

was decided for continuity to correct all of our spectral results to the origin bands determined by this earlier paper[5]. Theoretically, we could calibrate the laser before every run, but for an experiment for which a reference point is available, this seems unnecessarily time consuming. Alternatively, one might consider including some kind of reference in the sample with a known and simple fluorescence signature to which we could calibrate all spectra. However, it would be difficult to find a reference with a simple enough fluorescence pattern that it would not interfere with results.

Laser Induced Fluorescence Spectra

To produce the LIF spectrum, the dye laser was scanned using a Laser Photonics Digital Drive unit (Lscan1). A photomultiplier tube (Electron Tubes Limited, B2F/RP1) was optical coupled to the chamber to record the fluorescence output The PMT response was run through a boxcar integrator and read on the same PC described above. Fluorescence signals were visualized using an oscilloscope (Tektronix, 2236), and maximixed by tuning the laser to the most intensity transition and adjusting the beam until the maximum output was observed on the oscilloscope.

Reported LIF scans are the 4 co-added spectra with 60 shots per point, scanning at 0.01 nm increments. LIF scans were collected at a variety of backing pressures and nozzle distances in order to identify hot bands and clusters, but the final reported LIF scan was at an X/D of 21, and a helium backing pressure of 30 psi, which was determined by comparison to contain the least cluster or hot band activity, for the easiest analysis.

Since the power of the laser output at different wavelengths varied considerably, we also obtained power scans, in which the laser was tuned out of the gas pulse and

scattered off the valve face and the intensity was measured with the same photomultiplier tube. This was performed for both regions of the scan, and each scan was normalized with respect to the power of the laser, so that the intensity ratios would only reflect the intensities of the transitions, not of the laser itself.

Single Vibronic Level Fluorescence Spectrum

For SVLF scans, the dye laser is set at a fixed wavelength, to excite the molecules to a single vibronic level in the S_1 state. At Swarthmore, we were able to acquire SVLF spectra with the laser set to the wavelengths of the syn and anti origin bands. These wavelengths were determined using the LIF scan. The signal was then visualized on the oscilloscope, and the wavelength of the laser was adjusted to maximize the output power.

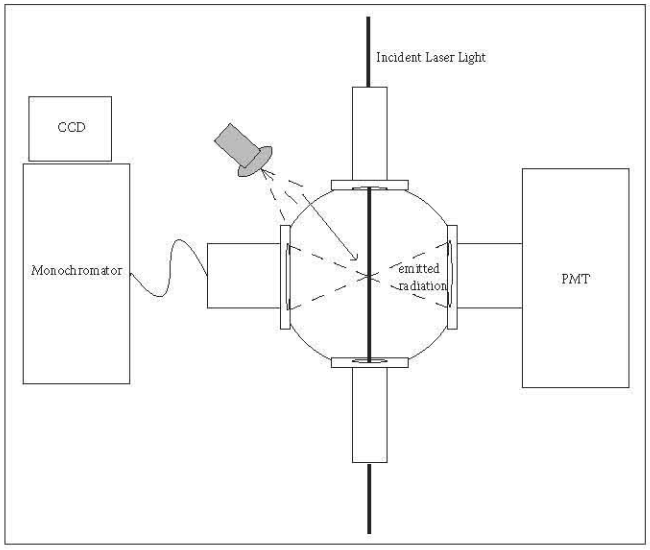

Figure 5. A schematic representation of the experimental set-up for both LIF and SVLF spectroscopy, as shown from above the vacuum chamber

To record the actual spectra, the molecular fluorescence was directed, using fiber optic cables, into the same monochromator and CCD setup described above, which was connected to the same PC for read-out. 5 minute acquisitions were taken in pairs and corrected spatially for cosmic rays. This process was repeated 16 times, and the resulting spectra were co-added. Any remaining peaks less than 3 pixels wide were manually removed as they were assumed to be cosmic rays. A schematic of the experimental set-up is shown in Figure 5.

Purdue Spectra

It was impossible to acquire SVLF spectra of any other bands using our equipment due to low power of the nitrogen pump laser. Additional SVLF spectra were acquired in the lab of Timothy Zwier at Purdue University. An LIF spectrum was also acquired at Purdue to ensure consistency. However, the power of the laser in this set-up proved to be so intense that many of the LIF transitions were saturated, making intensity information less reliable than the Swarthmore set-up, but giving better signal-to-noise (S/N) than the less powerful set-up. Both LIF spectra were used for analysis, since the better S/N of the Purdue spectrum allowed for the analysis of low intensity peaks. The saturation of the peaks in the LIF spectrum taken at Purdue, however, does not change the reliability of the SVLF intensity data, since the fluorescence from each transition is dispersed, thus giving each peak in the SVLF considerably lower intensity.

As at Swarthmore, all spectra were collected under jet-cooled conditions. Gaseous anethole was heated in a sample chamber and helium was passed through the sample chamber and through a pulsed valve (General Valve, Series 9) with a 800 μm orifice into an evacuated chamber.

The design of the chamber used at Purdue was slightly different than the one used at Swarthmore, in that this chamber employed 2 spherical mirrors, which increased the efficiency of fluorescence collection. The collected light could then be directed to either a PMT (for LIF scans) or to a monochromator (0.75 m, JY 750i, 2400 grooves/mm) and a CCD (Andor DH720) (for SVLF scans). The excitation source was frequency-doubled,

Nd:YAG pumped, dye laser (Lambda Physik Scanmate 2E. A more complete description of this experimental set up can be found in references ([36,37])

Computational Details

To supplement and assist in assigning experiment spectra, ground state optimization and frequency calculations of the syn and anti conformer of anethole were run at the Hartree-Fock (HF)[23- 22], Density-Functional Theory-B3LYP (DFT-B3LYP)[10,11], and Moller-Plesset Second Order (MP2)[20-21] levels of theory, at the 6-31G(d), 6-31G(d,p), 6-311G+(d,p), and 6-311G++(d,p)[13-12] basis sets. Calculations at the B3LYP/6-311G++(d,p) level of theory showed the planar geometry that has been shown in many styrene derivatives[9,5,24, 38,34]. As will be show in the spectral analysis, a planar geometry is most favored and therefore B3LYP calculations were used to assist in assignments primarily.

Calculations were run at the default convergence criteria. Additionally, a "very-tight" convergence criteria was investigated, but was abandoned after yielding very similar results with significantly more computing time.

Additionally, configuration-interaction singles (CIS)[17] optimizations were performed for the first 3 excited singlet states of both the syn conformer. All CIS calculations were done with the 6-311G(d,p) basis set, as basis sets including diffuse functions would not converge. Time dependent-DFT/B3LYP[39-40] calculations were also performed at the 6-311g++(d,p) basis set.

Single point energy CIS and TD-DFT calculations were performed for the first 3 excited singlet states of the syn conformer from the optimized ground state geometry for the 6-31G(d), 6-31G(d,p), 6-311G+(d,p), and 6-311G++(d,p) basis sets.

Most calculations were also performed for trans-β-methylstyrene and anisole in order to determine how comparable these two molecules were. All calculations were performed using Gaussian09 software[41]. We employed the resources of GridChem[42,43] due to the high computational cost of these calculations.

Results

Calculations

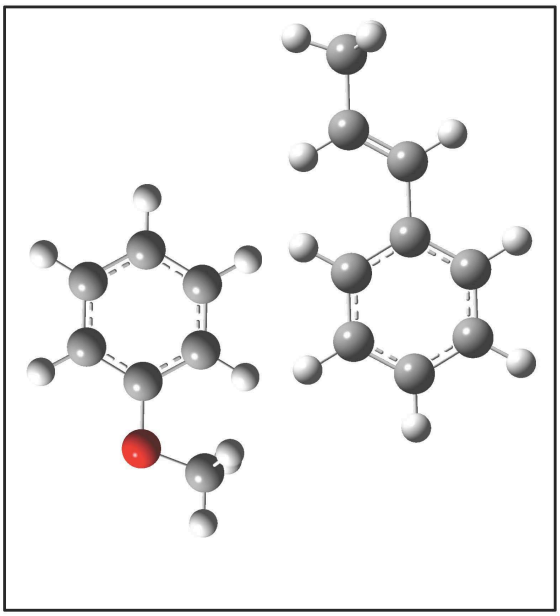

Figure 6. DFT-B3LYP 6-311++g(d,p) optimized structures of anisole (left) and *trans*-β-methylstyrene (right)

Optimization and frequency calculations were run for both *syn* and *anti* anethole using Gaussian 09[41], at a variety of basis sets and levels of theory. Additionally, the same set of calculations was run for anisole and *t*βms (see figure 6). A complete list of calculations is given in the experimental section. The goal of these calculations was to first provide a starting point for the assignment of spectra, and second to determine whether a comparison between the vibrations of these molecules is actually valid.

Grassian et al[5]. concluded that the vinyl group of anethole and other styrene derivatives is planar based on electronic excitation spectroscopy, using time of flight mass spectrometry for detection. Styrene itself, and many other styrene-like systems exhibit planar geometry including *trans*-β-methylstyrene[18,44], anisole[26], paravinyl phenol[38], and 4-methoxystyrene[27]. Anisole has also been shown to be planar by both microwave spectroscopy[45] and later by electronic spectroscopy[26]. All these previous results suggest that anethole should exhibit C_s symmetry. However, when C_s symmetry constraints were placed on anethole, optimization calculations would not converge to a

stable minimum. Therefore, a study was undertaken to determine the basis set that gave a geometry closest to planar. The results of these calculations are shown in Table 1.

Table 1. Energies calculated using Gaussian for Syn and Anti Anethole, Anisole, and Trans-B-Methylstyrene, with the angles from planarity of the vinyl group, except for anisole, where the angle is the methoxy dihedral.

	Syn-Anethole							
Level of Theory	6-31g(d)		6-31g(d,p)		6-311+g(d,p)		6-311++g(d,p)	
	energy (a.u.)	Angle (°)	energy (a.u.)	Angle (°)	energy (a.u.)	Angle (°)	energy (a.u.)	Angle (°)
Hartree Fock	-460.5045566	24.238	-460.5247543	25.098	-460.6158296	24.083	460.6159947	24.34
DFT-B3LYP	-463.4905939	0.024	-463.5082865	0.025	-463.6161915	0.024	-463.6162863	0.024
MP2	-461.9527843	29.122	-462.0488663	29.243	-462.2223021	31.523	-462.2230826	31.817
	Anti-Anethole							
Level of Theory	6-31g(d)		6-31g(d,p)		6-311+g(d,p)		6-311++g(d,p)	
	energy (a.u.)	Angle (°)	energy (a.u.)	Angle (°)	energy (a.u.)	Angle (°)	energy (a.u.)	Angle (°)
Hartree Fock	-460.5047631	17.682	-460.5249469	19.081	-460.616079	14.902	-460.6162438	14.649
DFT-B3LYP	-463.4908442	0.001	-463.5085377	0.003	-463.6164933	0.003	-463.6166334	0.003
MP2	-461.9528731	26.299	-462.0489515	26.706	-462.2222042	29.094	-462.2229952	29.433
	Anisole							
Level of Theory	6-31g(d)		6-31g(d,p)		6-311+g(d,p)		6-311+++g(d,p)	
	energy (a.u.)	Angle (°)	energy (a.u.)	Angle (°)	energy (a.u.)	Angle (°)	energy (a.u.)	Angle (°)
Hartree Fock	-344.5832617	0.017	-344.5969591	0.029	-344.6682623	0.03	-344.6683684	0.031
DFT-B3LYP	-346.7713208	0.019	-346.7833185	0.016	-346.8675653	0.016	-346.8676462	0.016
MP2	-345.6466455	0.019	-345.7094988	0.018	-345.8430465	0.026	-345.8435143	0.026
	Trans-β-methylstyrene							
Level of Theory	6-31g(d)		6-31g(d,p)		6-311+g(d,p)		6-311++g(d,p)	
	energy (a.u.)	Angle (°)	energy (a.u.)	Angle (°)	energy (a.u.)	Angle (°)	energy (a.u.)	Angle (°)
Hartree Fock	-346.6247267	23.163	-346.6419824	24.055	-346.704905	21.851	-346.7050177	22.009
DFT-B3LYP	-348.9680437	0.043	-348.9833158	0.006	-349.0602105	0.008	-349.0603037	0.015
MP2	-347.7648334	28.794	-347.8447348	28.964	-347.9633899	31.443	-347.9640766	31.722

The ideal choice for a basis set and level of theory is one that gives the lowest energy, and that gives a geometry most close to planar for the vinyl group. DFT-B3LYP[10,11] calculations showed a geometry much closer to planar than either Hartree-Fock[22-23] or MP2[20-21] calculations. It was found that the basis set had very little effect on the angle out of plane of the vinyl group, but that higher basis set calculations, as expected, showed a lower energy, suggesting that the calculations were converging to the

lowest energy at these higher basis sets. Therefore, DFT-B3LYP calculations were treated as the most accurate S_0 state calculations in determining geometry and vibrational modes, and were used throughout this study as the standard to which experimental results could be compared.

An approximate description of each calculated normal mode of both syn and anti anethole can be found in table 2 along with their calculated and, when available, experimental frequencies. The vibrations of *trans*-β-methylstyrene (*t*βms) and anisole were also examined, and qualitatively matched up with their counter-parts in the set of anethole vibrations. Vibrational motions of each normal mode were visualized side by side in GaussView and modes with the most similar motion were matched up qualitatively. The result of this matching is shown in table (vibration comparison). Vibrations are numbered according to the Mulliken numbering scheme.[1] Experimental studies of trans-β-methylstyrene[18] and anisole[26] also exist and the calculations gave us a better idea of which vibrations in the experimental studies were comparable to vibrations in anethole. The results of this vibrational comparison are shown in table 3. The comparison with previous work proved to be quite helpful in many peak assignments. A good example of this is in the assignment of multiple quanta of the 63^0_2 vibration of anethole. In *t*βms[18], as well as in styrene[19,46], a large anharmonicity of the torsional potential is evident. Therefore, in looking for multiple quanta of the ν_{63}, one cannot simply multiply the frequency of one quanta. In *t*βms, for example, 2 quanta of the vinyl torsion appear at 67 cm^{-1}, while 4 quanta appear at 155 cm^{-1}, a full 21 cm^{-1} greater than the 2 quanta of the vibration doubled. Prior knowledge of this anharmonicity thus allowed us to assign multiple quanta of ν_{63} in anethole, even though they appeared

significantly higher than a harmonic potential would predict in both conformers. Prior work is also useful when calculations predict that 2 different assignments are possible. For example, the transition at 0^0_0 -380 could feasibly be either the 38^0_1 or the $39^0_1 63^0_2$. However, based on the spectrum of *t*βms[18], we should see the ν_{38}, since the corresponding transition in the *t*βms spectrum, the 27^0_1, is quite intense.

Additionally, a calculation at the B3LYP/6-311g++(d,p)[10,11] level was also performed for the ground state of benzene. Styrene derivatives have been shown elsewhere to exhibit benzene- like vibrational modes[9,18, 26], and this calculation was used to compare vibrational modes to benzene. Benzene-like vibrations are therefore also numbered in Table 2 with the Wilson numbering scheme[15]. Some important vibrations (vibrations that appear frequently in the spectroscopy) are shown in Figure 7.

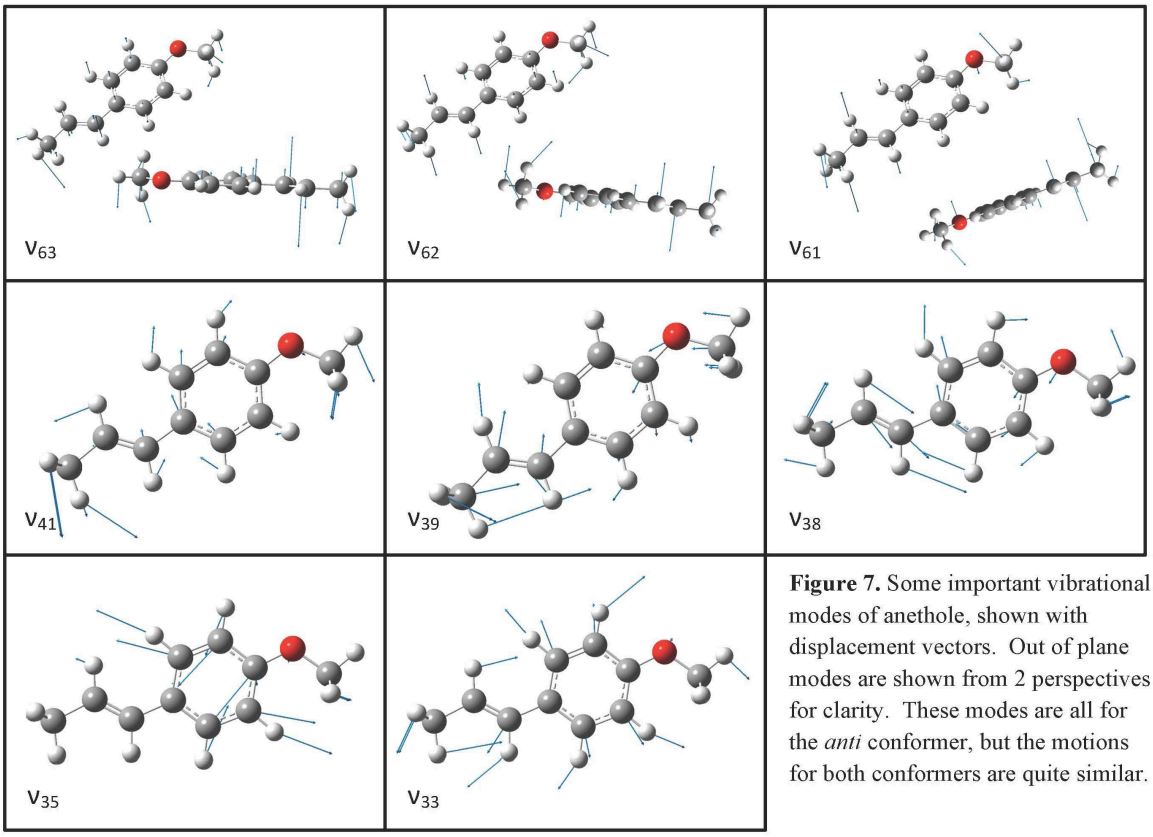

Figure 7. Some important vibrational modes of anethole, shown with displacement vectors. Out of plane modes are shown from 2 perspectives for clarity. These modes are all for the *anti* conformer, but the motions for both conformers are quite similar.

Table 2. Vibration frequencies with Mullikan numbers[1] and approximate descriptions for the S0 state. Benzene-like modes are additionally labeled in parenthesis using the Wilson numbering scheme. α, in plane ring angle bend; β, in plane bend; γ, out of plane bend. Numbers and letters in parenthesis in describtions refer to carbon labels

Mulliken Number	Syn Anethole Frequency				Anti Anethole Frequency				Approximate description in S_0
	S_0	S_1	S_0	S_1	S_0	S_1	S_0	S_1	
					a"				
63	29		29.42	32.58	33		35.63	39.05	C(1)-C(α) torsion
62	68		73.52	75.61	76		77.68	67.9	C(4)-O torsion
61	110	88	112.84	102.44	109	82	114.54	76.01	γ C(4)-O
60			185.81	129.92			185.67	131.05	methyl torsions
59			206.75	179.13			206.32	141.72	methyl torsions
58	246		250.71	207.52			248.63	182.13	O-C(δ) torsion + C(δ)H stretch
57			387.93	301.03			386.47	269.92	γ C-C=C + C-O-C)
56 (16a)			422.35	339.99			426.71	319	Ring deform
55 (16b)			526.05	400.36			527.91	382.75	X-Sens ring puckering
54 (10b)			726.1	520.52			727.05	513.12	X-Sens ring deform
53 (11)			807.25	646.92			802.36	622.39	Vinyl + aryl γCH
52 (10a)			812.82	675.57			822.48	648.33	aryl γCH
51			858.12	698.78			854.5	702.16	vinyl + aryl γCH
50			937.41	809.17			939.51	808.91	vinyl + aryl γCH
49 (17a)			965.25	830.26			965.86	824.72	aryl γCH
48			995.12	910.58			995.78	889	vinyl γCH
47			1062.89	1007.86			1062.82	1006.85	γ C-C-H
46			1168.27	1158.85			1166.35	1152.23	γ O-C-H
45			1478.64	1459.7			1478.52	1457.9	γ H-C(γ)-H
44			1492.85	1485.62			1491.08	1488.07	γ H-C(δ)-H
43			3044.72	2991.37			3045.3	2994.56	C(γ)H asymmetric stretch
42			3061.06	3075.34			3060.57	3078.74	C(δ)H asymmetric stretch
					a'				
41	121	130	123.24	129.52*	124	131	125.45	129.66	β C-C=C
40			248.85	249.25			242.08	244.41	β C-O-C
39	325	307	326.78	323.25	318	307	318.66	316.95	β C=C-C + C-O-C
38	380		383.25	383.2	410	392	409.99	396.2	X-sens (αC-C-C)
37			500.68	493.87			472.9	468.39	β C=C-C + C-O-C
36	569		569.96	550.76	581		586.6	572.73	X-Sens (αC-C-C)
35 (6b)	651		651.37	609.33	644	585	652.48	604.62	αC-C-C
34	767	654	770.54	761.27			766.13	744.72	X-Sens C(1)-C(α) + C(4)-O stretch
33(1)	849		852.21	825.45	847		851.51	826.4	X-Sens Ring Breath
32			957.03	937.03			957.16	928.67	vinyl β C-H
31 (18a)			1023.79	974.34			1023.44	972.74	aryl β CH + ring C-C stretch
30 (18b)	1063		1061.13	1035.56			1061.36	1038.58	aryl β CH + ring C-C stretch
29			1111.25	1095.51			1111.18	1087.44	aryl β CH + vinyl β CH
28 (15)			1137.32	1129.22			1138.22	1106.8	aryl β CH
27 (9a)			1195.96	1147.71			1197.35	1135.04	aryl β CH
26			1201.55	1195.53			1202.31	1192.18	β O-C-H
25	1233		1232.02	1242			1234.86	1228.54	aryl β CH + vinyl β CH
24	1268		1276.73	1254.92			1271.49	1256.86	aryl β CH + C(4)-O stretch
23			1311.32	1282.59			1310.61	1271.8	vinyl β C-H
22			1330.93	1317.62	1323		1329.84	1315.94	aryl β CH + vinyl β CH
21 (14)			1339.82	1339.31			1341.13	1345.93	X-Sens ring C-C stretch
20 (19b)			1363.18	1369.27			1364.17	1371.98	X-Sens ring C-C stretch
19			1413.34	1394.82			1414.47	1391.28	C(γ)H symmetric stretch
18 (19a)			1448.42	1423.94	1432		1450.34	1405.03	ring C-C stretch
17			1476.94	1447.25			1473.84	1441.24	C(δ)H symmetric stretch
16			1492.08	1469.15			1493.18	1468.02	C(γ)H bend
15			1505.07	1477.03			1504.38	1475.15	C(δ)H bend
14			1542.59	1499.09			1542.11	1499.89	X-sens ring C-C stretch
13 (8b)			1607.13	1505.97			1607.59	1504.77	ring C-C stretch
12 (8a)			1648.71	1547.47			1649.03	1539.72	ring C-C stretch
11			1709.16	1571.79			1708.24	1570.7	C(α)=C(β) stretch
10			3003.19	2975.23			3002.85	2977.04	C(δ)H symmetric stretch
9			3005.76	3014.19			3006.22	3017.41	C(γ)H symmetric stretch
8			3087.44	3087.86			3088.23	3089.19	C(γ)H stretch
7			3112.73	3141.51			3113	3139.73	C(α)H stretch
6			3131.46	3142.75			3132.52	3139.91	C(β)H stretch
5			3132.04	3163.39			3132.87	3162.66	C(δ)H stretch
4			3160.09	3178.71			3159.99	3183	aryl CH stretch
3			3175.62	3196.65			3174.23	3188.07	aryl CH stretch
2			3191.02	3213.12			3192.58	3223.64	aryl CH stretch
1			3202.43	3229.27			3202.23	3235.78	aryl CH stretch

Table 3. calculated vibrational frequencies at the B3LYP/6-311++G(d,p) level for Syn and Anti Anethole, Anisole, and Trans-B-Methylstyrene. Frequencies are given in cm^{-1}. Vibrations are listed in the table so that normal modes with similar motions are listed on the same row. In some cases, two different modes appeared to be possible matches, in which case the vibration number, and frequency, of the second mode is also shown in the adjacent column. Vibrations are numbered according to the Mulliken Scheme.

Syn Anethole		Anti Anethole		Anisole			Trans-β-methylstyrene		
Number	Frequency	Number	Frequency	Number	Frequency	Other modes	Number	Frequency	Other Modes
				a''					
63	29.42	63	35.63				51	37.8	
62	73.52	62	77.68						
61	112.84	61	114.54	42	90.57		50	124.96	
60	185.81	60	185.67						
59	206.75	59	206.32	41	205.12		49	195.54	
58	250.71	58	248.63	40	267.11		48	288.43	
57	387.93	57	386.47						
56	422.35	56	426.71	39	422.72		47	412.95	
55	526.05	55	527.91	38	516.78		46	511.25	
54	726.1	54	727.05				45	703.08	
53	807.25	53	802.36	37	703.28		44	752.73	
52	812.82	52	822.48	35	823.98				
51	858.12	51	854.5	36	764.71		43	835.08	42, 849.58
50	937.41	50	939.51	34	890.29		41	925.59	
49	965.25	49	965.86	33	964.74		40	979.82	
48	995.12	48	995.78	32	983.63		39	991.4	38, 1003.03
47	1062.89	47	1062.82				37	1063.95	
46	1168.27	46	1166.35	31	1166.55				
45	1478.64	45	1478.52				36	1478.64	
44	1492.85	44	1491.08	30	1492.07				
43	3044.72	43	3045.3				35	3047.99	
42	3061.06	42	3060.57	29	3060.67				
				a'					
41	123.24	41	125.45				34	152.9	
40	248.85	40	242.08						
39	326.78	38	409.99				33	350.29	
38	383.25	39	318.66	28	256.64		32	411.42	
37	500.68	37	472.9	27	445.79				
36	569.96	36	586.6	26	560.35		31	626.48	
35	651.37	35	652.48	25	629.18		30	634.27	
34	770.54	34	766.13	24	797.34				
33	852.21	33	851.51				29	833.61	
32	957.03	32	957.16	23	1009.35		28	956.41	
31	1023.79	31	1023.44	22	1040.86		27	1014.84	
30	1061.13	30	1061.36	21	1065.36		26	1050.37	
29	1111.25	29	1111.18	20	1101.84		25	1096.68	
28	1137.32	28	1138.22	19	1178.43		24	1122.72	
27	1195.96	27	1197.35	18	1194.3		23	1181.85	
26	1201.55	26	1202.31	17	1201.49		22	1205.18	
25	1232.02	25	1234.86				21	1231.67	
24	1276.73	24	1271.49	16	1271.41				
23	1311.32	23	1310.61				20	1306.58	
22	1330.93	22	1329.84	15	1335.06		19	1333.74	
21	1339.82	21	1341.13	14	1356.79		18	1352.64	
20	1363.18	20	1364.17				17	1366.67	
19	1413.34	19	1414.47				16	1414.04	
18	1448.42	18	1450.34				15	1476.62	
17	1476.94	17	1473.84	13	1473.34				
16	1492.08	16	1493.18				14	1493.57	
15	1505.07	15	1504.38	11	1506.02	12, 1485.15			
14	1542.59	14	1542.11	10	1526.66		13	1526.29	
13	1607.13	13	1607.59	9	1624.29		12	1614.76	
12	1648.71	12	1649.03	8	1641.87		11	1648.71	
11	1709.16	11	1708.24				10	1709.16	
10	3003.19	10	3002.85	7	3003.06				
9	3005.76	9	3006.22				9	3008.08	
8	3087.44	8	3088.23				8	3091.09	
7	3112.73	7	3113				7	3116.5	
6	3131.46	6	3132.52				6	3134.17	
5	3132.04	5	3132.87	6	3132.48				
4	3160.09	4	3159.99	5	3163.47		5	3156.16	
3	3175.62	3	3174.23	4	3171.1	3, 3186.96	4	3162.75	
2	3191.02	2	3192.58	2	3194.56		3	3172.67	
1	3202.43	1	3202.23	1	3202.42		2	3181.08	

Table 4. Summary of energies from excited state optimization, as compared to the energy calculated from the same basis set for the ground state.

	basis set	syn anethole	anti anethole
HF energy (a.u.)	6-311g(d,p)	-460.61045	-460.61071
CIS energy (a.u.)		-460.42283	-460.41985
Difference (a.u.)		0.18762	0.19086
difference (cm-1)		41177.83008	41888.92788
DFT/B3LYP energy (a.u.)	6-311++g(d,p)	-463.61629	-463.61663
TDDFT/B3LYP energy (a.u.)		-463.46323	-463.46580
Difference (a.u.)		0.15306	0.15083
difference (cm-1)		33592.78687	33103.35844

Since the spectroscopy also gives information about the S_1 state, we ran additional optimization and frequency calculations on the excited states of both conformers using time dependent DFT-B3LYP (TD-DFT)[39-40] using the same 6-311++g(d,p) basis set. For comparison, we also ran CIS[17] calculations on both conformers. Generally, DFT calculations do a better job of predicting geometries, but other levels of theory do better at predicting energy differences. It was found that CIS calculations did not converge using diffuse functions in the basis set description, but did converge without diffuse functions , behavior that has been seen in other calculation studies[38]. The results of CIS calculations are therefore shown at the 6-311g(d,p) basis set, alongside HF calculations at the same basis set for comparison. CIS calculations must be compared to HF calculations at the same basis set, as the wavefunctions used for these calculations are derived from the HF wavefunctions with the promotion of a single electron to an excited state[47]. The results of all excited state energy calculations are summarized in Table 4 and the calculated vibrational modes for the TD-DFT calculations are included in Table 2.

The optimization and frequency excited state calculations turn out to be of limited use, since they do not calculate vibrational frequencies accurately enough to be useful in determining assignments of experimentally observed transitions in the LIF. Furthermore, their applicability is limited when talking about the energetics of the excited state as

compared to the ground. The movement of electrons is significantly faster than the relaxation of the nuclei into their optimized conformation. In fact, the Born-Oppenheimer approximation states that the nuclear positions of the atom remain unchanged during an electronic transition More likely, the excitations observed experimentally are vertical excitations, that is, they are an excitation of an electron to an excited state that has almost the same geometry as the ground state. Therefore, we also ran a series of single point energy excited state calculations: energy only TD-DFT and CIS calculations run for the geometry determined in the ground state optimization of the relevant level of theory (DFT and HF, respectively). The results are shown in Table 5.

Table 5. Ground state and excited state energies calculated using Gaussian09. CIS calculations are done as single point energy calculations using the optimized geometry of the HF calculation at the same basis set. TD-DFT calculations are done as single point energy calculations using the optimized geometry of the DFT calculation at the same basis set. Δ is the difference between the ground and excited states.

		Syn Anethole		Anti Anethole		Anisole		*Trans*-β-methylstyrene	
		HF/CIS	DFT/ TD-DFT	HF/CIS	DFT/ TD-DFT	HF/CIS	DFT/ TD-DFT	HF/CIS	DFT/ TD-DFT
S (a.u.)	6-31g(d)	-460.50456	-463.49059	-460.50476	-463.49084	-344.58326	-346.77132	-346.70502	-348.96804
S_1 (a.u.)		-460.29248	-463.32138	-460.29189	-463.32009	-344.35420	-346.58045	-346.40829	-348.78876
Δ (a.u.)		0.21208	0.16921	0.21288	0.17076	0.22906	0.19087	0.29673	0.17929
Δ (cm^{-1})		46546	37137	46721	37477	50273	41891	65124	39349
S (a.u.)	6-31g(d,p)	-460.52475	-463.50829	-460.52495	-463.50854	-344.59696	-346.78332	-346.70490	-348.98332
S_1 (a.u.)		-460.31274	-463.33942	-460.31208	-463.33824	-344.36822	-346.58045	-346.42560	-348.80438
Δ (a.u.)		0.21202	0.16887	0.21287	0.17030	0.22874	0.20287	0.27930	0.17894
Δ (cm^{-1})		46533	37062	46720	37376	50202	44524	61299	39272
S (a.u.)	6-311+g(d,p)	-460.61583	-463.61619	-460.61608	-463.61649	-344.66826	-346.86757	-346.64198	-349.06021
S_1 (a.u.)		-460.41604	-463.45644	-460.41518	-463.45441	-344.44865	-346.68316	-346.49992	-348.88895
Δ (a.u.)		0.19979	0.15975	0.20089	0.16208	0.21961	0.18441	0.14206	0.17126
Δ (cm^{-1})		43848	35061	44091	35573	48199	40473	31179	37587
S (a.u.)	6-311++g(d,p)	-460.61599	-463.61629	-460.61624	-463.61663	-344.66837	-346.86765	-346.62473	-349.06030
S_1 (a.u.)		-460.41627	-463.45656	-460.41550	-463.45456	-344.44878	-346.68326	-346.50009	-348.88906
Δ (a.u.)		0.19973	0.15973	0.20074	0.16208	0.21959	0.18438	0.12464	0.17125
Δ (cm^{-1})		43835	35056	44057	35572	48195	40467	27355	37585

The isomerization of the two conformers of anethole is also of interest. Potential energy scan calculations were run at a DFT and MP2 levels of the theory at the 6-

311g++(d,p) for both isomerization coordinates and are shown in Figure 8a (for the vinyl torsion) and 8b (for the methoxy torsion). The same calculations were additionally run for the methoxy torsion of anisole and the vinyl torsion of *t*βms. The results of these calculations were fit to the truncated Fourier series[9]

$$V(\varphi) = \frac{1}{2}\sum_{n=1}^{4} V_n[1 - \cos(n\varphi)]$$

Only the v_1, v_2, and v_4 terms were included in the fit, as the v_3 term was expected to be insignificant in accordance with previous work.[9] This same work ignored the v_1 term as well, but for anethole, since the two isomers exhibit slightly different energies, some odd v term is necessary to account for the difference in the barriers. We have chosen to use the v_1 term but in principle any odd v_n would have the same effect[27]. the v_1 term is necessary to achieve a reasonable fit. v_1 represents the difference in the barrier heights depending on the starting isomer, v_2 the lowest barrier height, and v_4 the anharmonicity of the potential. The results of these fits are shown in Table 6.

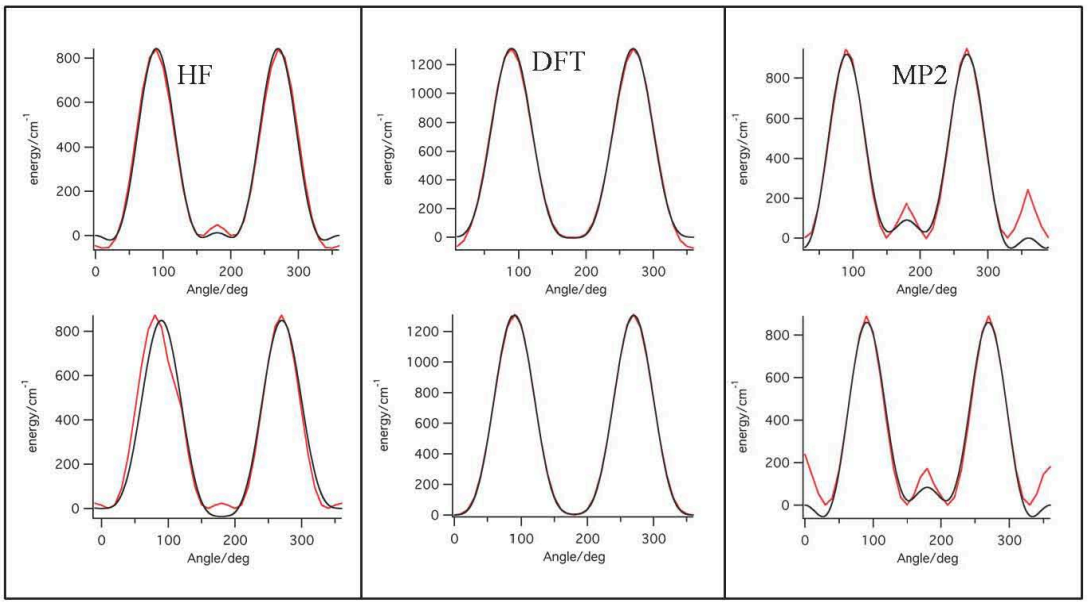

Figure 8a. potential energy scans of the vinyl rotation at 3 different levels of theory, each using the 6-311++g(d,p) basis set for anethole (top) and *t*βms (bottom). The calculations are performed by stepping the vinyl dihedral angle through 360 degrees, and re-optimizing the rest of the structure at each step. Calculation data is shown in red. Each scan is also fit to the truncated Fourier transform (equation 1). Fits are shown in black, and the parameters of each fit are listed in Table 7.

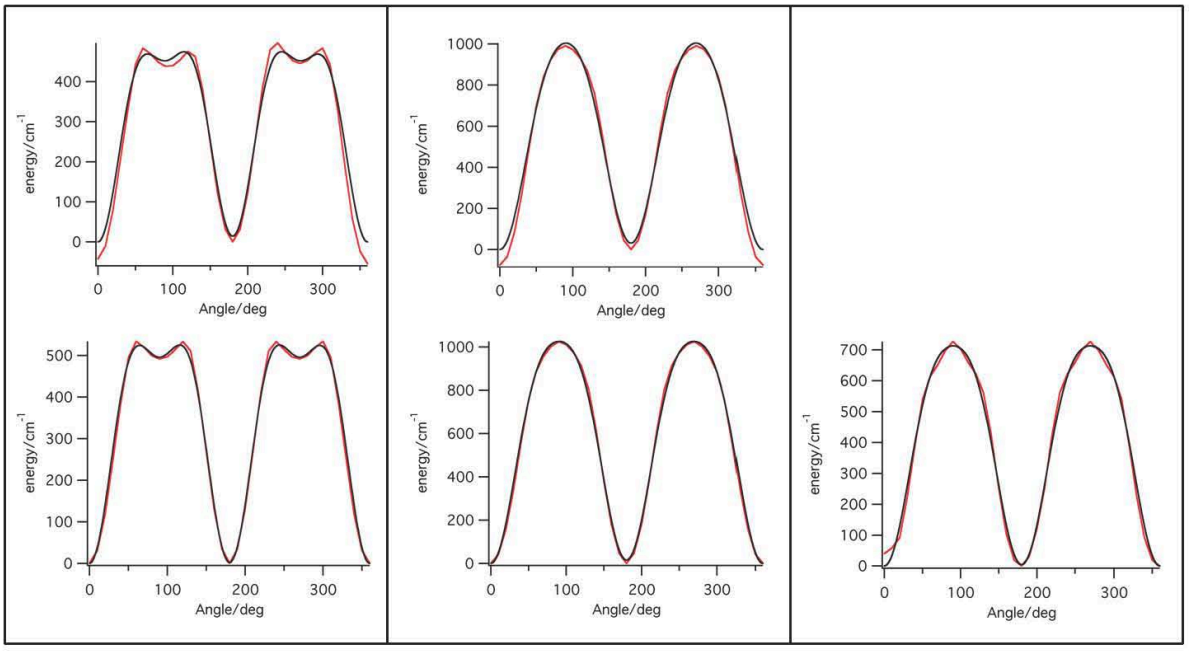

Figure 8b. Potential energy scans of the methoxy rotation at 3 different levels of theory, each using the 6-311++g(d,p) basis set for anethole (top) and *t*βms (bottom). The calculations are performed by stepping the methoxy dihedral angle through 360 degrees, and re-optimizing the rest of the structure at each step. Calculation data is shown in red. Each scan is also fit to the truncated Fourier transform (equation 1). Fits are shown in black, and the parameters of each fit are listed in Table 7.

Table 7. Fit parameters for the vinyl and methoxy scans of anethole, as well as the vinyl scan of *t*βms. Calculated from the Fourier transform described in eq. 1.

		V1/cm-1	uncertainty	V2/cm-1	uncertainty	V4/cm-1	uncertainty
	HF	12.56	11.6	836.926	11.6	-286.82	11.6
	DFT	5.72	10.8	1314.9	10.8	-313.05	10.8
Anethole Vinyl	MP2	90.821	26.4	873.67	25.9	-359.37	26.4
	HF	14.048	11.5	444.85	11.5	169.26	11.5
	DFT	30.768	16.4	988.96	16.4	103.4	16.4
Anethole Methoxy	MP2						
	HF	2.3131	5.29	494.8	5.29	199.69	5.29
	DFT	15.468	7.36	1018.5	7.36	156.61	7.36
Anisole Methoxy	MP2	4.522	8.66	710.68	8.66	105.47	8.66
	HF	36.346	24.6	867.81	24.6	-203.9	24.6
Trans-β-methylstyrene	DFT	5.5585	1.81	1302.6	1.81	-291.67	1.81
Vinyl	MP2	83.839	30.1	817.38	30.1	-346.59	30.1

Spectral Results

The laser-induced fluorescence (LIF) spectrum of jet-cooled anethole is shown in Figure 9 and is partially assigned. Assigning the LIF spectrum is easiest when the amount of congestion is minimized. To minimize congestion, hot bands, as well as Van der Waals clusters with the carrier gas must be avoided. In order to make the LIF spectra as simple as possible, we undertook a pressure study. We varied the backing pressure of the carrier gas and the position of the valve in order to determine the configuration that minimized hot bands but maximized the signal to noise ratio. The results of this study are shown in Figure 10.

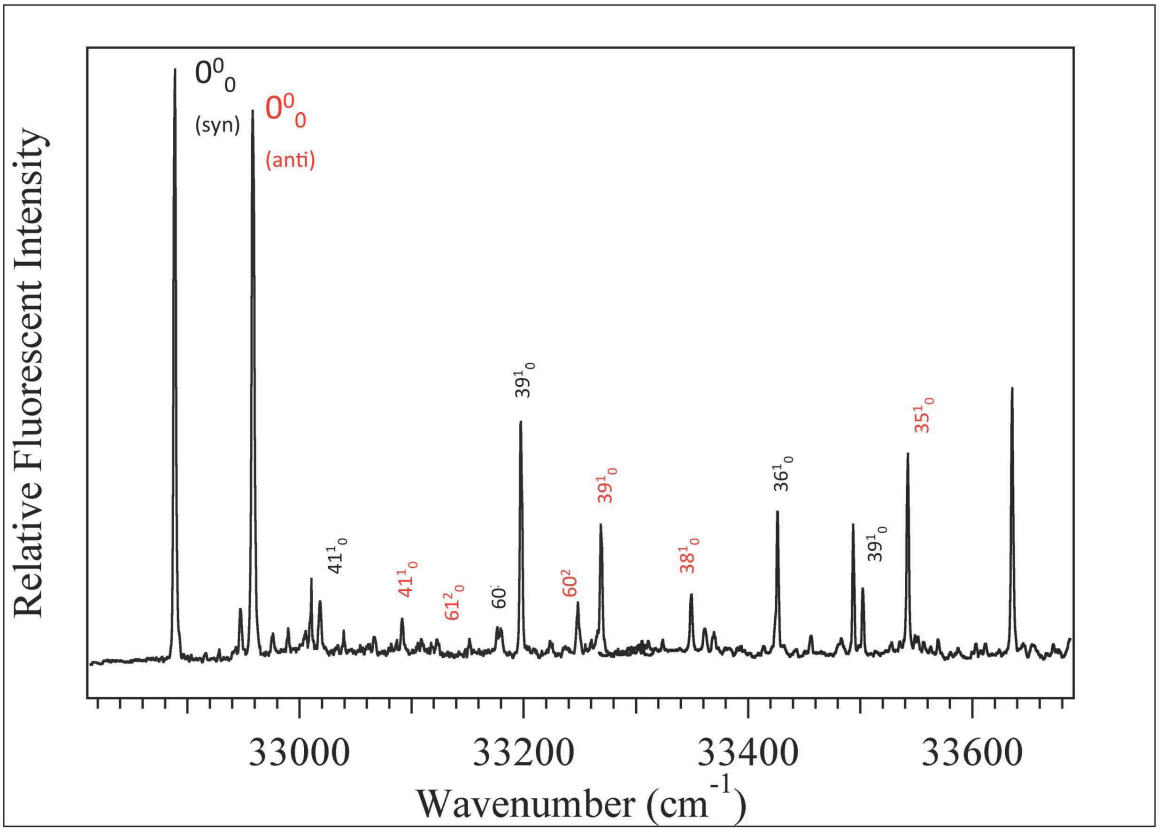

Figure 9. jet-cooled LIF spectrum of anethole, in wavenumbers, with some transitions labeled. Transitions labeled in red originate from the anti conformer, while those in black originate from the syn conformer.

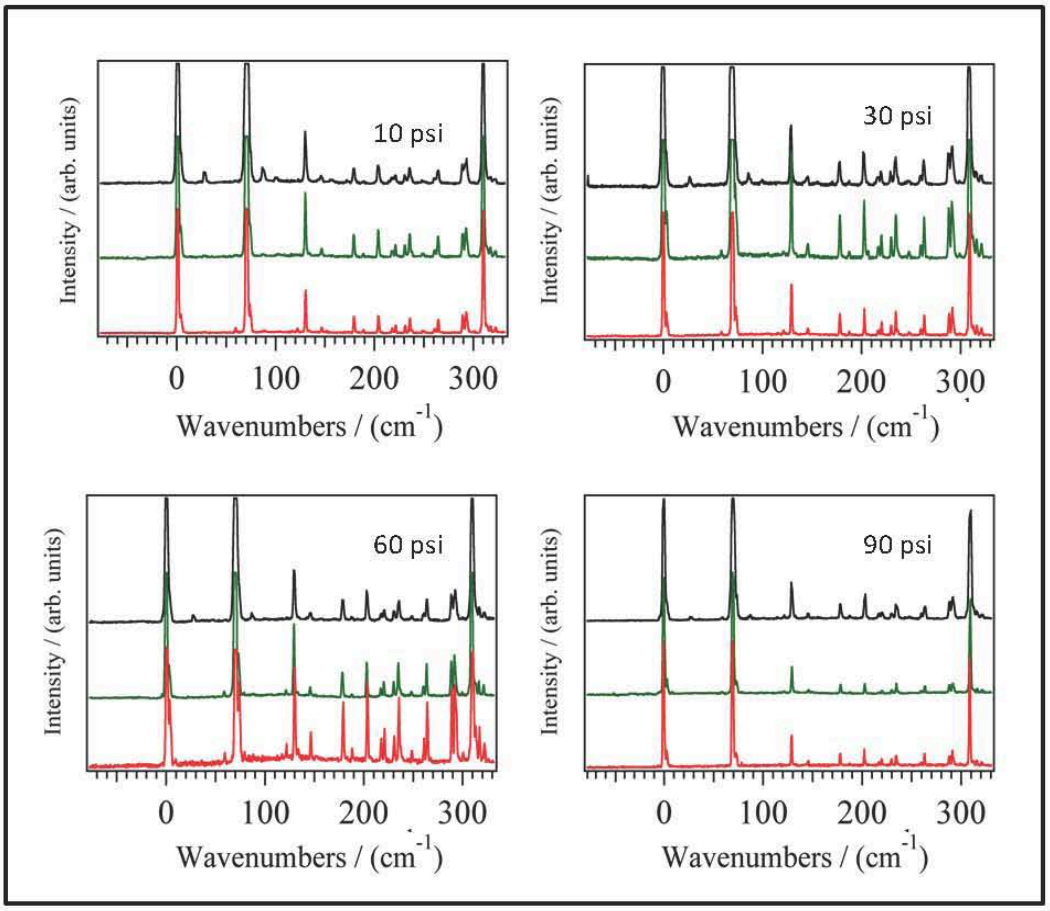

Figure 10. LIF scans of the origin region at a verity of He backing pressures and valve location (x/D, where x is the distance from the valve face to the point of intersection with the laser pulse, and D is the diameter of the orifice). Black, x/D=7, Green, x/D=21, Red, x/D=42. Wavenumbers are relative wavenumbers from the syn origin at 32889 cm^{-1}

For x/d of 7, we can see a small peak growing in just to the right of the syn origin, at 26 cm^{-1} above the syn origin. This band is likely a hot band, the result of the laser interacting with the jet before it is completely cooled. The spectra at 60 psi and 30 psi, and at 42 and 21 x/d look almost the same. However, in the spectra at 60 psi, there is evidence of a small peak to the left of the first intense transition at 121 cm^{-1} above the syn origin, likely due to a cluster between anethole and water (the identity of this peak is discussed further later in this work). At 90 psi, the jet becomes to diffuse and we begin to lose signal. We therefore chose to use 60 psi and x/d=21 for the rest of our experiments, since it kept a good signal to noise ratio but minimized hot bands and clusters.

Table 8. partial assignments of the LIF spectrum of anethole, noting the conformer each transition belongs to where available. [a]$\Delta v = v - v(0_0^0)$ of the relevant conformer.

wavenumber (cm^{-1})	conformer	assignment	Δv^a (cm^{-1})
32889.00	syn	0_0^0	0
32947.84	syn	H_2O	58.84
32958.70	anti	0_0^0	0
32977.72	syn	H_2O	88.72
33009.84	anti	H_2O	51.14
33018.01	syn	41_0^1	129.01
33033.83			
33038.74	anti	H_20	106.8
33065.50	syn	61_0^2	176.5
33074.80			
33090.12	anti	41_0^1	131.12
33104.91			
33108.2	syn		219.2
33117.52			
33122.45	anti	61_0^2	163.45
33129.04			
33135.62			
33147.71			
33151.00	syn		262
33175.75	syn	61_0^4	286.75
33178.50	syn		
33196.12	syn	39_0^1	307.12
33202.74			
33207.70			
33221.49			
33235.29			
33245.79	anti	61_0^4	287.79
33253.52			
33256.84			
33265.69	anti	39_0^1	306.69
33285.62			
33294.49			
33297.82			
33303.36			
33306.69			
33318.90			
33325.56			
33351.12	anti	38_0^1	392.12
33363.36			
33372.27	syn		483.27
33385.64			
33429.16	syn	36_0^1	540.16
33495.23			
33503.08	syn	39_0^2	614.08
33543.54	anti	35_0^1	654.54

Table 9. assignment of part of the SVLF spectrum following excitation into the 0_0^0 band of the anti conformer at 32889 cm^{-1}. [a]$\Delta\nu=\nu(0_0^0)$ - ν_F where ν_F is the frequency of the flourescence.

$\Delta\nu^a$ (cm^{-1})	assignment	$\Delta\nu^a$ (cm^{-1})	assignment	$\Delta\nu^a$ (cm^{-1})	assignment
0	0_0^0	870.14		1823.56	
58.38	63_2^0	894.09		1865.1	
96.92	$63_1^0 62_1^0$	909.04	$33_1^0 63_2^0$	1596.29	
122.04	41_1^0	948.59	$33_1^0 63_1^0 62_1^0$	1621.31	
131.45	63_4^0	970.93	$33_1^0 41_1^0$	1646.29	
139.28	$63_1^0 61_1^0$	979.11	$33_1^0 63_1^0 61_1^0$	1679.77	
167.47		991.02		1701.1	
175.29		1017.75		1720.28	
204.97	63_6^0	1063.7	30_1^0	1739.43	
241.61		1103.61		1759.27	
257.18		1174.31	$33_1^0 39_1^0$	1800.98	
276.62		1216.14	$33_1^0 38_1^0$	1823.56	
324.72	39_1^0	1232.99	25_1^0	1865.1	
352.59		1268.09	24_1^0	1913.54	
380.4	38_1^0 and $39_1^0 63_2^0$	1297.28	36_2^0	1926.16	
422.04	$39_1^0 63_1^0 62_1^0$	1342.42		1947.85	
455.12	$39_1^0 63_4^0$	1355.5	$36_2^0 63_2^0$	2005.1	
464.34		1389.61		2026.69	
491.97	58_2^0	1417.13		2067.69	
505		1429.43		2085.72	
526.44	$39_1^0 63_6^0$	1499.41	$33_1^0 39_2^0$	2117.58	
569.23	36_1^0	1541.82		2146.6	
587.54		1553.31		2170.06	
615.72		1596.29		2192.11	
626.37		1621.31		2027.25	
650.68	35_1^0	1646.29		2245.71	
703.75		1679.77		2268.33	
739.28		1701.1		2281.34	
770.21		1720.28			
819.12		1739.43			
833.39		1759.27			
849.15	33_1^0	1800.98			

Table 10. assignment of part of the SVLF spectrum following excitation into the 000 band of the anti conformer at 32958 cm-1. a$\Delta\nu$=ν(000) - vF where vF is the frequency of the fluorescence.

$\Delta\nu^a$ (cm^{-1})	assignment	$\Delta\nu^a$ (cm^{-1})	assignment	$\Delta\nu^a$ (cm^{-1})	assignment
0	0_0^0	957.81	$33_1^0 63_1^0 62_1^0$	1642.38	
64.95	63_2^0	974.26	$33_1^0 41_1^0$	1661	
109.16	$63_1^0 62_1^0$	989.94	$33_1^0 63_4^0$	1678.87	
124.92	41_1^0	1016.8		1686.74	
142.24	$63_1^0 61_1^0$	1054.03	59_2^0	1704.59	33_2^0
154.03	63_4^0	1062.21		1736.67	
189.37		1080.04		1748.77	
211.32		1106		1753.75	
222.29		1134.14		1771.53	
235.6		1151.15		1804.89	
247.33	63_6^0	1168.14	$33_1^0 39_1^0$	1816.23	
256.71		1185.86		1845.96	
317.53	39_1^0	1196.18		1865.05	
355.62		1207.23		1882.69	
382.79	$39_1^0 63_2^0$	1219.75		1905.25	
409.9	38_1^0	1234.46		1918.63	
427.69		1257.24	$33_1^0 38_1^0$	1933.41	
445.47		1280.71		1949.58	
473.25	$38_1^0 63_2^0$	1298.3		1983.96	
496.36		1313.67		2007.08	
519.44		1323.18	22_1^0	2012.67	
553.23		1342.91		2022.47	
580.83	36_1^0	1361.88		2048.31	
617.55		1385.21		2070.64	
644.27	35_1^0	1408.5		2080.39	
708.23	$35_1^0 63_2^0$	1432.48	18_1^0	2092.23	
726.46	$38_1^0 39_1^0$	1493.35		2099.88	
762.09		1515.04		2106.84	
811		1526.59		2129.77	
830.11		1538.86		2149.89	
847.45	33_1^0	1574.16		2179.84	
873.79		1601.48		2284.53	
912.1	$33_1^0 63_2^0$	1621.97		2328.46	
949.57		1630.91		2455.43	

For some bands, while specific assignments could not be determined , we were able to determine whether they arose from the syn or anti conformer. These assignments, along with specific band assignments are indicated where available are listed in Table 8. In order to assign these bands, the SVLF spectra of the excitation of many of the bands were collected and examined.

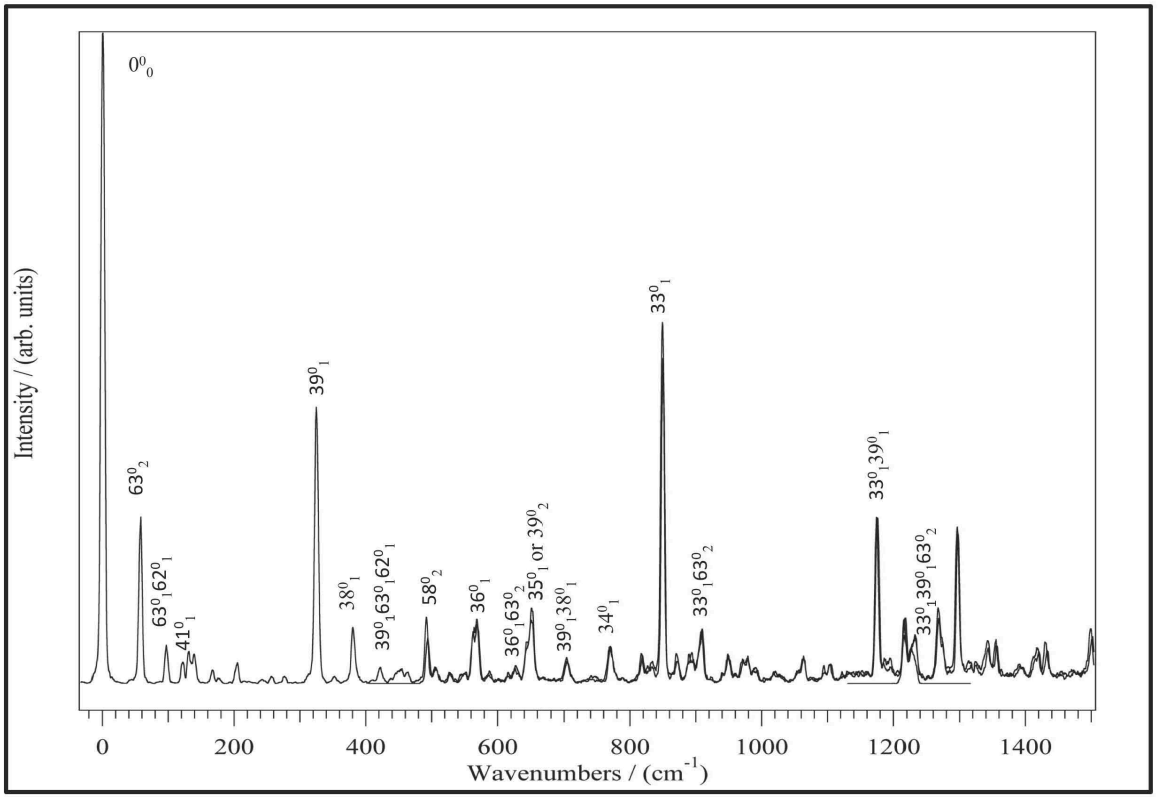

Figure 11. SVLF spectrum of the syn conformer origin band. Shown in relative wavenumbers to the excitation at 32889cm^{-1}. Transitions are labeled according to the Mulliken numbering scheme[1]

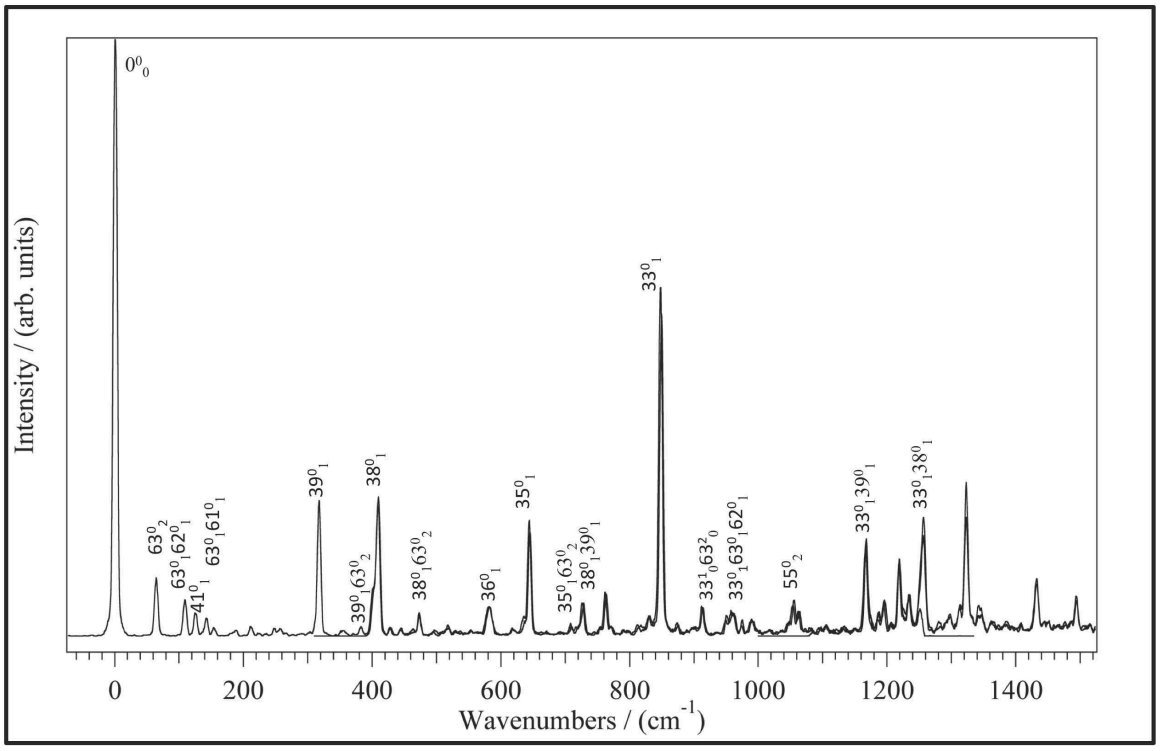

Figure 12. SVLF spectrum of the anti conformer origin band. Shown in relative wavenumbers to the excitation at 32889cm^{-1}. Transitions are labeled according to the Mulliken numbering scheme[1]

SVLF spectra were assigned where possible based on comparison calculations, and previous works on similar molecules including 4-methoxystyrene[27], *para*-vinylphenol[38], anisole[26]and *trans*-β-methylstyrene[18,44]. The simplest SVLF spectra arise from excitation of the origin bands, at 32889 cm^{-1} and 32958 cm^{-1}. The frequencies and assignments of these spectra are shown in Tables 9 and 10. The spectra are shown with assignments in figures 11 and 12**.** Based on the frequencies of the observed bands in the SVLF these spectra were assigned to the syn and anti conformer origins, respectively. Grassian et. al[5] had previously assigned these bands to the same conformers, and this work confirms this assignment based on the high intensity of these bands, and their location on the red end of the LIF spectrum. One important transition in the SVLF is the 63^0_2 transition, which corresponds to the vinyl group torsional mode. This transition turns

out to be a good diagnostic of which rotamer we are looking at: In the syn conformer, this transition appears 57 cm^{-1} above the origin while in the anti conformer it appears 65 cm^{-1} above the origin. This transition is visible in most SVLF spectrum examined, and appears reliably at the same frequencies for each conformer. Another useful diagnostic transition is the 39^0_1 transition, which corresponds to the in-plane bending of the C=C-C and the C-O-C bonds. This transition is quite intense and also appears reliably in most spectra at a relative wavenumber of 325 cm^{-1} for the syn conformer and 317 cm^{-1} for the anti conformer.

Several other additional SVLFs were acquired as well. The assignments of these SVLF spectra, where available, are included in Table 11 and their corresponding spectra are shown in Figures 13-15. Generally, the highest intensity observed band in the spectrum was assigned to the transition from some number of quanta of a vibration in the excited state to the same number of quanta of the same vibration in the ground state, because it is expected that these two states will have the best Franck-Condon overlap. This transition is generally referred to as a false origin, and appears at a relative wavenumber that matches the calculated ground state frequency of a vibrational state, and the frequency of the corresponding transition in the origin SVLF spectra. The multiple comparisons are useful in making an assignment with a high probability of accuracy. Calculations and previous assignments of the origin band SVLF spectra were then used to assign other transitions. For bands that did not have one pronounced most intense band, the assignment process was a bit more complex, but through trial and error some of these SVLF spectra could also be assigned.

There were also some bands in the LIF spectrum could not be assigned to any transition of either conformer. We hypothesized that these bands might belong to van der Waals clusters. The previously mentioned pressure study was used to eliminate the possibility of anethole:He clusters, but water clusters have been shown to exist for a similar systems. Water clusters have been observed in anisole, in which the water hydrogen bonds with the oxygen, and in benzene and styrene, in which the hydrogens of water interact with the π orbitals above and below the ring.[34,30] SVLF bands of these unidentified bands (see Figures 16 and 17) also suggested that these bands did not belong to simple anethole, because there are transitions visible below the frequency of the usual 63_2^0 transition, which was the lowest transition observed in all other spectra, which also suggested that these bands were not from anethole alone. To verify that these transitions belonged to water clusters, water was added in a separate cell to the gas line and kept at a temperature just above freezing, so as to keep the vapor pressure low. The result of this study is shown in Figure 18.

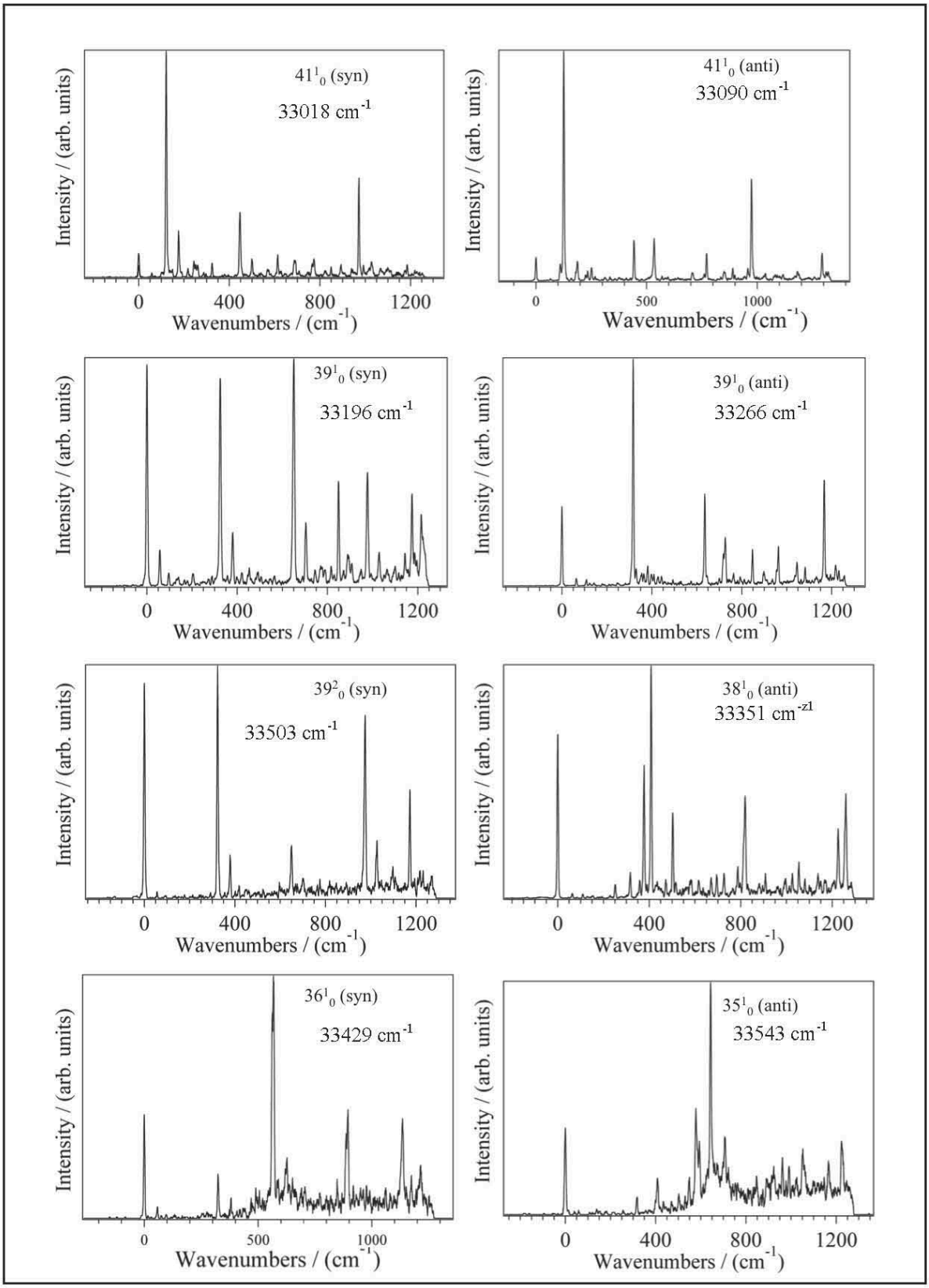

Figure 13. SVLF spectra that display false origin bands. These spectra are all of in-plane vibrational motions and do not include any combination bands or overtones. All spectra are given in wavenumbers relative to the excitation energy, which is shown on the spectra.

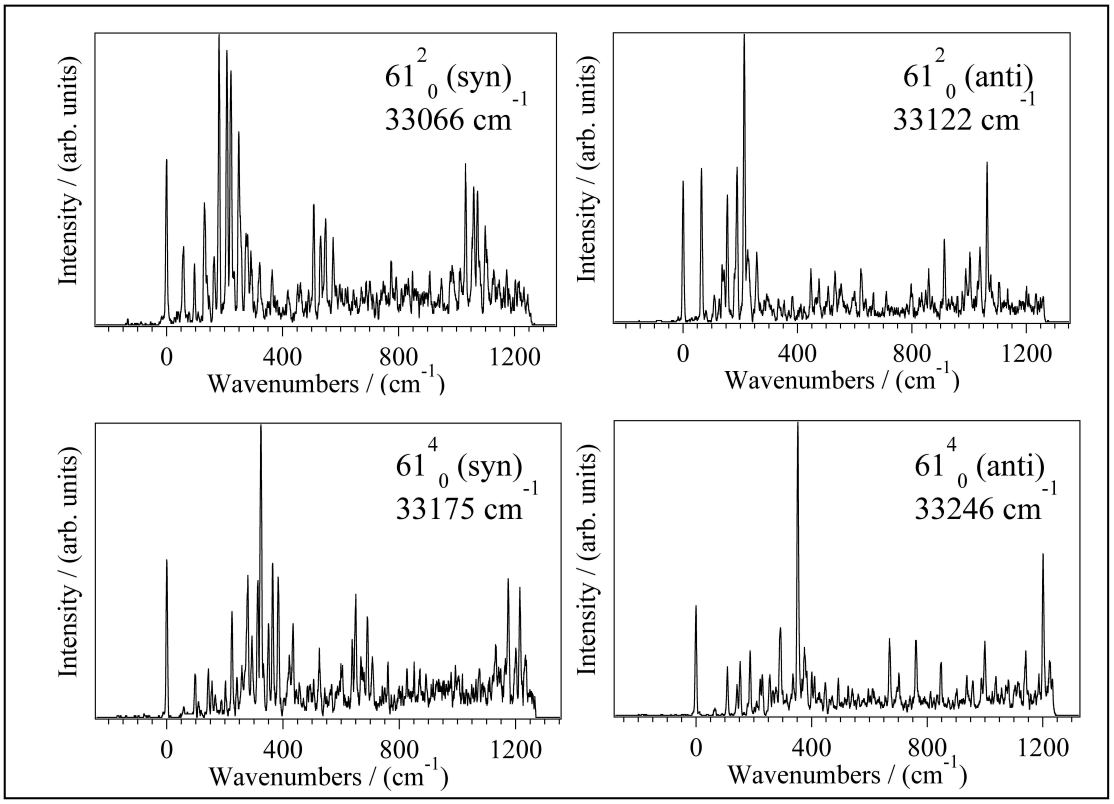

Figure 14. SVLF spectra tentatively assigned to the overtone bands of the v_{61} mode. All spectra are shown in relative wavenumbers to the excitation energy, which is shown on the spectra

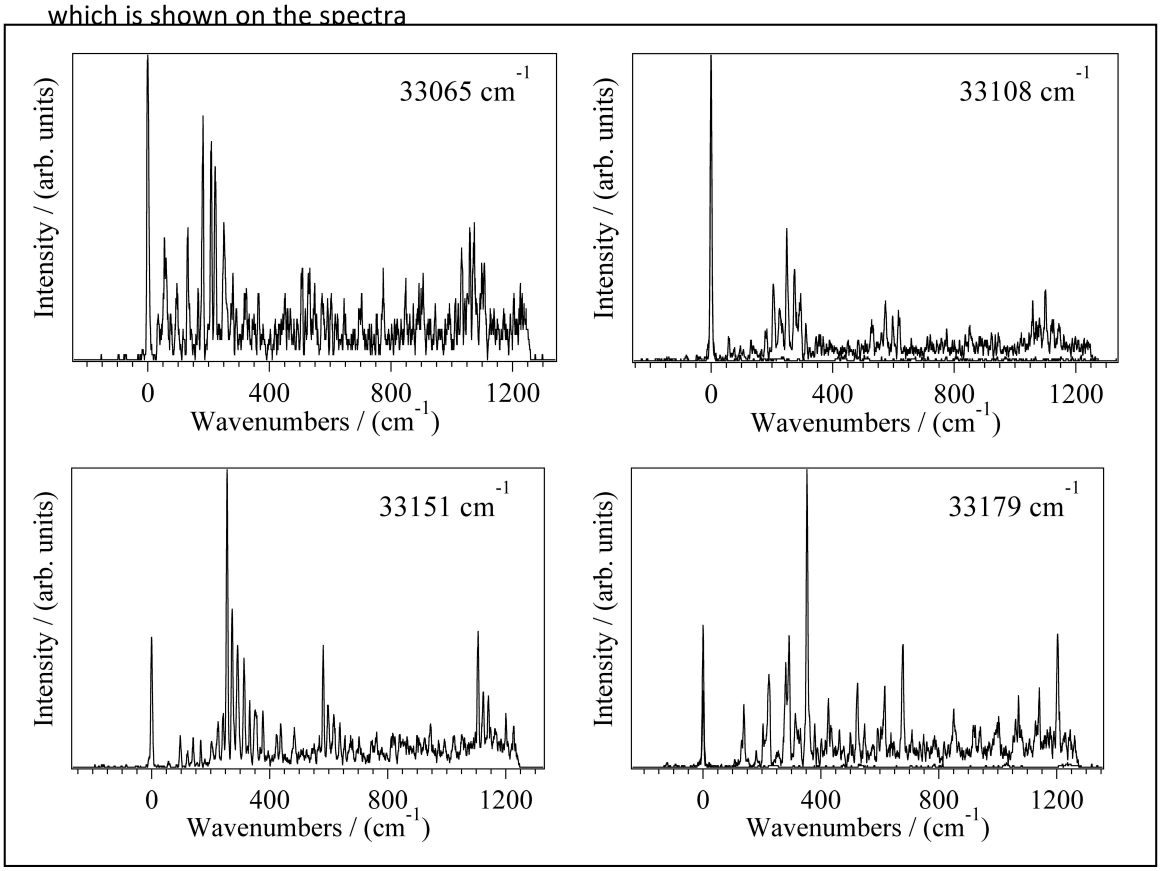

Figure 15. SVLF spectra that have not yet been assigned, and are likely due to combination bands. These spectra are all thought to arise from the syn conformer. They are all shown in relative wavenumbers to the excitation frequency, which is

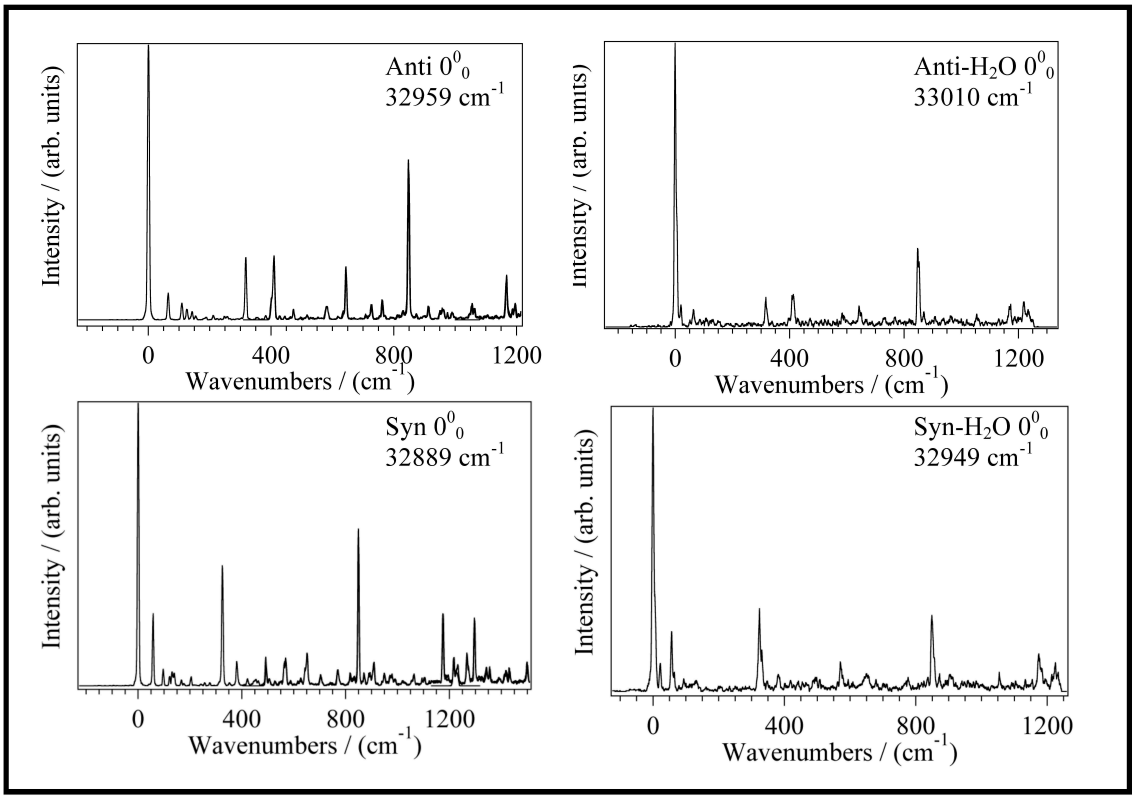

Figure 16. Top left: anti origin SVLF spectrum. Top right: suspected anti water cluster origin. Bottom left: syn origin SVLF spectrum. Top right: suspected syn water cluster origin. All spectra are in relative wavenumbers to the excitation energy, which is included on each spectrum.

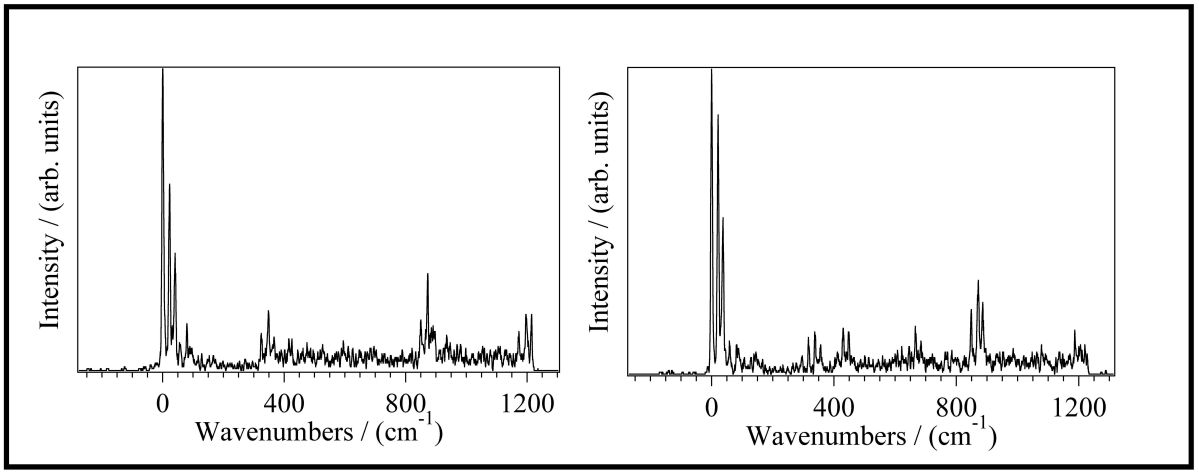

Figure 17. Two additional spectra thought to arise from syn-anethole and water clusters (left) and anti anethole and water clusters (right). Spectra in relative wavenumbers to the excitation energy, which is shown on each spectrum.

Table 11. Summary of the partial assignments of all SVLF spectra, where possible, for the both the syn and the anti conformer. In cases where the spectrum was only assigned in the low wavenumber region, the higher wavenumber peaks were not included in the table. [a]$\Delta\nu$ is the difference between the wavenumber of the transition and the excitation wavenumber.

Syn 0^0_0 +130 cm^{-1}, excitation in the 41^1_0		
Wavenumber/cm^{-1}	$\Delta\nu^a$	Assignment
33019	0	41^1_0
33077.83	58.83	$41^1_0\,63^0_2$
33126.18	107.18	$41^1_0\,62^0_1 63^0_1$
33140.41	121.41	41^1_1
33157.8	138.8	$41^1_0 61^0_1 62^0_1$
33168.85	149.85	
33194.88	175.88	$41^1_1 63^0_2$
33236.59	217.59	$41^1_1 62^0_1 63^0_1$
33262.51	243.51	41^1_2
33270.35	251.35	$41^1_1 62^0_2$
33278.98	259.98	$41^1_1 61^0_1 62^0_1$
33306.4	287.4	
33315.79	296.79	
33343.14	324.14	
33466.06	447.06	$39^0_1 41^1_1$
33517.91	498.91	$39^0_1 41^1_1 63^0_2$
33558.8	539.8	$39^0_1 41^1_1 62^0_1 63^0_1$
33588.83	569.83	

Syn 0^0_0 + 307 cm^{-1}, excitation in the 39^1_0		
Wavenumber/cm^{-1}	$\Delta\nu^a$	Assignment
33196	0	39^1_0
33253.87	57.87	$39^1_0 63^0_2$
33293.132	97.132	$39^1_0 62^0_1 63^0_1$
33336.3	140.3	
33362.62	166.62	
33374.57	178.57	
33399.24	203.24	
33469.87	273.87	
33485.7	289.7	
33521.26	325.26	39^1_1
33552.81	356.81	
33576.43	380.43	$39^1_1 63^0_2$
33595.3	399.3	
33615.72	419.72	$39^1_1 62^0_1 63^0_1$
33649.43	453.43	
33688.55	492.55	
33700.26	504.26	
33722.11	526.11	
33743.93	547.93	
33762.61	566.61	
33782.05	586.05	
33847.18	651.18	39^1_2
33899.71	703.71	$39^1_2 63^0_2$
33939.77	743.77	$39^1_2 62^0_1 63^0_1$
33965.91	769.91	
33983.57	787.57	
34013.47	817.47	
34026.48	830.48	

Anti 0^0_0 + 131cm^{-1}, excitation in the 41^1_0		
Wavenumber/cm^{-1}	$\Delta\nu^a$	Assignment
33090	0	41^1_0
33155.47	65.47	$41^1_0 63^0_2$
33200.03	110.03	$41^1_0 62^0_1 63^0_1$
33215.91	125.91	41^1_1
33250.02	160.02	
33270.6	180.6	
33276.93	186.93	$41^1_1 63^0_2$
33314.06	224.06	
33323.53	233.53	$41^1_1 62^0_1 63^0_1$
33341.66	251.66	41^1_2
33357.41	267.41	
33402.21	312.21	
33424.18	334.18	
33449.24	359.24	
33467.23	377.23	
33480.52	390.52	
33498.48	408.48	
33532.77	442.77	$39^0_1 41^1_1$
33568.56	478.56	
33624.4	534.4	$38^0_1 41^1_1$
33660.76	570.76	
33686.78	596.78	
33731.68	641.68	
33796.93	706.93	
33851.24	761.24	
33861.16	771.16	$35^0_1 41^1_1$
33925.9	835.9	
33940.33	850.33	
33979.77	889.77	
33988.86	898.86	
34047.81	957.81	
34064.39	974.39	$33^0_1 41^1_1$
34127.6	1037.6	$33^0_1\,41^1_1 63^0_2$
34207.7	1117.7	
34272.5	1182.5	
34383.7	1293.7	$33^0_1 39^0_1 41^1_1$
34402.2	1312.2	
34410.3	1320.3	

Anti 0^0_0 + 307 cm^{-1}, excitation in the 39^1_0		
Wavenumber/cm^{-1}	Δv^a	Assignment
33265.69	0	39^1_0
33328.63	62.94	$39^1_0 63^0_2$
33375.28	109.59	$39^1_0 62^0_1 63^0_1$
33596.27	330.58	
33620.82	355.13	
33629.52	363.83	
33647.7	382.01	$39^1_1 63^0_2$
33662.71	397.02	
33672.33	406.64	
33693.46	427.77	
33709.21	443.52	
33900.91	635.22	39^1_2
33983.94	718.25	
33992.45	726.76	$38^0_1 39^1_1$
34029.53	763.84	
34058.84	793.15	
34076.54	810.85	
34095.77	830.08	
34113.44	847.75	$39^1_1 55^0_1$
34164.04	898.35	
34222.1	956.41	
34228.2	962.51	39^1_3
34301.98	1036.29	
34311.09	1045.4	
34329.28	1063.59	
34347.45	1081.76	
34398.83	1133.14	
34432.74	1167.05	$33^0_1 39^1_1$
34483.09	1217.4	
34498.09	1232.4	

Anti 0^0_0 +392 cm^{-1} ,excitation in the 38^1_0		
Wavenumber/cm^{-1}	Δv^a	Assignment
33351	0	38^1_0
33414.27	63.27	$38^1_0 63^0_2$
33461.16	110.16	$38^1_0 62^0_1 63^0_1$
33603.44	252.44	
33668.94	317.94	
33708.75	357.75	
33728.63	377.63	
33741.33	390.33	
33759.58	408.58	38^1_1
33785.72	434.72	
33822.88	471.88	$38^1_1 63^0_2$
33853.66	502.66	$38^1_1 62^0_1 63^0_1$

Syn 0^0_0 + 614 cm^{-1}, excitation in the 39^2_0		
Wavenumber/cm^{-1}	Δv^a	Assignment
33503	0	39^2_0
33826.23	323.23	39^2_1
33882.43	379.43	$39^2_1 63^0_2$
33926.47	423.47	$39^2_1 63^0_1\ 62^0_1$
33948.84	445.84	$39^2_1\ 41^0_1$
33967.99	464.99	
34151.97	648.97	39^2_2
34205.5	702.5	$39^2_2 63^0_2$
34279.22	776.22	$39^2_2 63^0_1 62^0_1$
34321.42	818.42	
34394.62	891.62	
34477.55	974.55	39^2_3
34529.26	1026.26	$39^2_3 63^0_2$
34551.59	1048.59	
34570.05	1067.05	
34596.93	1093.93	
34650.56	1147.56	
34677.31	1174.31	$39^2_1 33^0_1$
34696.39	1193.39	
34716.2	1213.2	

Syn 0^0_0 + 540 cm^{-1}, excitation in the 36^1_0		
Wavenumber/cm^{-1}	Δv^a	Assignment
33429	0	36^1_0
33486.87	57.87	$36^1_0 63^0_2$
33752.42	323.42	$36^1_0 39^0_1$
33809.17	380.17	$36^1_0 38^0_1$
33836.28	407.28	
33850.61	421.61	
33871.3	442.3	
33898.3	469.3	
33934.77	505.77	
33949.02	520.02	
33955.35	526.35	
33995.64	566.64	36^1_1
34017.71	588.71	
34055.49	626.49	$36^1_1 63^0_2$
34079.84	650.84	
34119.83	690.83	
34135.48	706.48	
34201.06	772.06	
34229.87	800.87	
34248.52	819.52	
34276.47	847.47	
34316.75	887.75	
34324.48	895.48	$36^1_1 39^0_1$
34347.66	918.66	
34360.01	931.01	
34379.29	950.29	
34391.62	962.62	
34404.7	975.7	
34420.09	991.09	
34490.66	1061.66	
34509.02	1080.02	
34526.59	1097.59	
34563.97	1134.97	36^1_2
34580.72	1151.72	
34603.54	1174.54	
34643.78	1214.78	$36^1_1 35^0_1$

Anti 0^0_0 + 585 cm^{-1}, excitation in the 35^1_0			Syn 0^0_0 + 175 cm^{-1}, excitation in the 61^2_0		
Wavenumber/cm^{-1}	$\Delta\nu^a$	Assignment	Wavenumber/cm^{-1}	$\Delta\nu^a$	Assignment
33544	0	35^1_0	33065	0	61(2,0)
33862.37	318.37	$35^1_0 39^0_1$	33124	59	61(2,0)63(0,2)
33952.45	408.45	$35^1_0 38^0_1$	33161.37	96.37	61(2,0)62(0,1)63(0,1)
33978.1	434.1		33195.48	130.48	
34014.9	470.9		33229.52	164.52	
34046.83	502.83		33246.12	181.12	61(2,1)61(0,1)
34074.72	530.72		33272.96	207.96	
34093.82	549.82		33287.15	222.15	61(2,2)
34122.43	578.43	$35^1_0 36^0_1$	33313.92	248.92	
34138.3	594.3		33344.57	279.57	61(2,2)63(0,2)
34187.4	643.4	35^1_1	33355.56	290.56	
34215.06	671.06		33386.14	321.14	
34250.55	706.55	$35^1_1 63^0_2$	33429.17	364.17	
34267.08	723.08		33483.76	418.76	
34391.74	847.74		33517.21	452.21	
34419.83	875.83		33527.31	462.31	
34435.41	891.41		33554.47	489.47	
34467.32	923.32		33573.06	508.06	61(2,1)61(0,1)39(0,1)
34505.37	961.37	$35^1_1 39^0_1$	33596.28	531.28	
34521.65	977.65		33613.28	548.28	
34534.81	990.81		33639.52	574.52	
34553.4	1009.4		33662.64	597.64	
34569.6	1025.6		33670.34	605.34	
34596.6	1052.6	$35^1_1 38^0_1$	33681.89	616.89	
34603.6	1059.6				
34608.2	1064.2				
34642.1	1098.1				
34647.5	1103.5				
34664.4	1120.4				
34675.1	1131.1				
34678.2	1134.2				
34690.5	1146.5				
34709.6	1165.6				
34732.6	1188.6				
34737.9	1193.9				
34752.4	1208.4				
34767.7	1223.7	$35^1_1 36^0_1$			
Anti 0^0_0 + 163, excitation in the 61^2_0					
Wavenumber/cm^{-1}	$\Delta\nu^a$	Assignment	Wavenumber/cm^{-1}	$\Delta\nu^a$	Assignment
33122.45	0	61^2_0	33545.79	423.34	
33187.25	64.8	$61^2_0 63^0_2$	33569.21	446.76	$39^0_1 61^2_0 63^0_2$
33202.41	79.96		33597.26	474.81	
33231.1	108.65	$61^2_0 63^0_2$	33629.94	507.49	
33248.61	126.16	$41^0_1 61^2_0$	33653.23	530.78	$61^2_2 39^0_1$
33258.95	136.5		33675.72	553.27	
33265.3	142.85		33722.93	600.48	
33277.22	154.77	$61^2_1 63^0_1$	33743.78	621.33	
33311.33	188.88	$61^2_1 62^0_1$	33761.52	639.07	
33336.67	214.22	61^2_2	33776.16	653.71	
33348.53	226.08	$61^2_1 63^0_3$	33788.48	666.03	
33379.34	256.89	$39^0_1 61^2_0 63^0_2$	33833.05	710.6	
33414.81	292.36		33904.28	781.83	
33455.7	333.25				
33476.11	353.66				
33505.12	382.67				
33534.07	411.62				

Discussion

Assignment of origin band SVLFs (syn and anti).

The assignment of the origin band SVLF spectra of both the syn and the anti conformer proved to be essential in determining which origin belonged to which conformation. Firstly, these spectra confirmed that the bands they arose from were in fact two separate origin bands: the most intense peak in the SVLF is coincident with the excitation frequency, suggesting that this vibrational level in the ground state and the excited state have good wavefunction overlap (according to the Franck-Condon principle).. For SVLF, we expect that the transition with the largest intensity arises from the transition from some number of quanta in the excited state of a vibration to the same number of quanta in the ground state. Since the origin arises from zero quanta of any vibration, it is expected that the peak corresponding to the laser resonance for the origin (i.e., the peak in which the molecule falls from the zero point level in the S_1 state to the zero point level in the S_0 state) will be of highest intensity. Secondly, the experimental frequencies of the ground state vibrations in the SVLF spectra generally agree within 5 cm^{-1} with the calculated frequencies for each conformer.

The SVLF spectra also confirm that both conformers are planar. For all a" (out of plane) vibrations, the electric dipole selection rule[14] says that only even combinations or overtones will have appreciable intensity. This matches what is observed in the spectra. However, these transitions, (somewhat unsurprisingly, since they are combinations and overtones) tend to be much weaker than the a' transitions, and thus are quite difficult to pick out of the spectra.

The two origin SVLFs share some features in common. In both, the highest energy transition (the one closest to the laser resonance) is the 63^2_0. In the syn conformer this appears at 0^0_0 - 58 and in the anti conformer at 0^0_0 - 65 cm^{-1}. Next, both spectra exhibit a barely resolved group of 4 peaks. In the syn conformer, a peak at 0^0_0 - 96.92 cm^{-1} is attributed to the combination of one quantum each of the ν_{63} and the ν_{62} vibration. The anti conformer exhibits this same peak at 109.16.

Both spectra also show a small peak that can be attributed to one quantum of the ν_{41}, at 0^0_0- 122 cm^{-1} for the syn conformer and 0^0_0 - 124 cm^{-1} for the anti conformer, in good agreement with calculated frequencies for these modes of 123 and 125 cm^{-1}, respectively. There is an additional peak that can be assigned in both conformers to a combination of one quantum each of the ν_{63} and ν_{61} vibrations, at 0^0_0-139 cm^{-1} and 0^0_0-142 cm^{-1} for the syn and anti conformers, respectively. This leaves one band in the region near the origin in each spectrum that, based on calculations, cannot reasonably be assigned to any combination of low frequency modes. Based on the observed anharmonicity of the vinyl torsional mode in styrene and other styrene derivatives, including *t*βms[18], PVA[9], 4MEOSTY, it is likely that the 63^0_4 transition will have a significantly higher frequency than two times the 63^0_2 vibration. It is therefore reasonable to assign this last low frequency transition (at 0^0_0- 131 and 0^0_0 - 154 cm^{-1} for the syn and anti conformers, respectively, to 4 quanta of the ν_{63} mode.

Another prominent modes that appears in both SVLF's are the ν_{39}, one quantum of which appears at 0^0_0- 325 cm^{-1} for the syn conformer and 0^0_0- 318 cm^{-1} for the anti conformer. The ν_{39} is quite intense in both conformers, though it has a higher relative intensity in the syn spectrum. In both spectra, however, we also see theν_{39} mode

combined with additional vibrations. This effect is easier to see in the anti conformer, because in the syn conformer the $39^0_1 38^0_1$ and the $39^0_1 63^0_2$ are likely coincident in the band at 0_0^0 - 380.4.

One quantum of the ν_{38}, at 0^0_0- 380 and 0^0_0-410 cm^{-1} for the syn and anti, respectively, and the ν_{33}, at 0^0_0- 849 and 0^0_0-847 cm^{-1} for the syn and anti, respectively are also prominent transitions. The ν_{33} is the most intense transition in both spectra apart from the 0^0_0. The ν_{38} is easier to see in the anti spectrum, since, as mentioned previously, it coincides with another transition in the sin spectrum.

In general, the spectra both exhibit the same behavior of a few quite intense bands, that exhibit origin-like behavior, with vibrations built off of them. Most of these more intense peaks are readily identified from calculation results, and are verified where possible by comparison with *t*βms[18]. These bands tend to be in-plane stretching and bending modes, several of which involve the ring, which is to be expected for a conjugated, substituted benzene[9].

There are, however, obvious differences in these two spectra, both in terms of the frequencies of the modes, and in the intensities. For example, in the syn spectrum, the 63^0_2 vibration is almost two times more intense compared to the origin. In the anti conformer, the 39^0_1 is considerably more intense than the 38^0_1, while in the syn conformer, they are almost the same intensity. These differences reinforce the conclusion that these spectra belong to the same transition of two conformers of the same molecule.

Assignment of the LIF spectrum

The LIF spectrum of anethole presents a challenging case, because it is essentially 2 spectra superimposed on one another: one belonging to the syn and the other to the anti conformer. Furthermore, the TD-DFT calculations are not sufficiently accurate to help with the assigning process. Therefore, most of the assignment of the LIF is done by examination of the SVLF's produced from the LIF bands. The goal with each of these SVLFs is two-fold: firstly, to identify which conformer (and hopefully which vibration) the SVLF was produced from, and secondly, to examine the vibrational structure of the SVLF itself. In general the SVLF spectra fall into two categories. Some SVLFs exhibit "false origin" behavior. In these cases, one, strong peak dominates the spectrum, and most of the peaks are to the red of this one peak, much like in the origin band. This false origin peak is typically shifted from the laser resonance by a frequency that corresponds with the frequency of the vibration of the excitation in the S_0 state, and is assigned to the transition from 1 quanta of that vibration in the S_1 to one quanta of that vibration in the S_0. The SVLF spectra that exhibit this "false origin behavior," or come very close to this behavior, are shown in figure 15. Some SVLFs, however, are much more complex. These more complex spectra tend not to be dominated by one very strong peak, or the strongest peak in the spectrum is not the easily assigned transition from 1 quantum in the excited state to one quantum in the ground state. These spectra typically arise due to combination bands, overtone bands, or from modes that are very different in the S_1 state than in the S_0[9,18].

We have not yet been able to assign the 63^2_0 vibration in the LIF, but also cannot say that it is not present. This torsion was observed in *t*βms[18], styrene[24], and (E)-PVA[9], and is therefore likely present and just has not been found yet.

"False Origin" SVLFs

The easiest to see example of this behavior is in the SVLF spectrum of the LIF transition at 33265.69 cm^{-1}, (anti 0^0_0 + 307) which has been assigned to the 39^1_0 of the anti conformer. This spectrum is dominated by a very intense transition at 317 cm^{-1} below the excitation frequency, which is assigned to 39^1_1. The only peaks at higher frequencies are 3 very weak transitions. These transitions are assigned to vibrations built off of the laser resonance frequency, and exhibit almost exactly the same pattern as the anti origin SVLF, but much weaker. The transition 63 cm^{-1} below the laser resonance in particular is diagnostically useful, since it corresponds to the 63^2_0 transition frequency of the anti conformer, as observed in the anti origin SVLF at 65 cm^{-1}.

Following the false origin, we again see at least part of that same series of small peaks, in particular a peak 382 cm^{-1} below the excitation frequency. This peak is 65 cm^{-1} lower than the false origin peak, and is therefore assigned to the $39^1_1 63^2_0$ transition. The 39^1_1 peak is so intense that we are able to see 2 additional overtones of the peak. Additionally, some of the more intense peaks that were visible in the anti origin band can also be seen as combinations with the false origin, including the ν_{38} and the ν_{33}.

Very similar behavior is seen for SVLF of the band at 33196, which through the same process is assigned to the 39^1_0 transition of the syn conformer, but with some differences. Firstly, the peak at the laser resonance shows a much higher intensity for the

syn conformer than the anti conformer. Additionally, in the syn conformer spectrum, the 63^0_2 vibrations that are combined with the other vibrations are at a much higher relative intensity than those in the anti conformer. This is consistent with the origin spectra, which also showed that the syn 63^0_2 had a higher intensity than the same transition in the anti conformer spectrum. Additionally, the SVLF of the syn conformer shows a stronger progression of the ν_{39}, with almost no change in intensity up until the 39^1_3 and a still clearly visible 39^1_4 transition. We have also collected the SVLF of the 32^2_0 transition of the syn conformer, which, rather unsurprisingly, looks very similar to that of the 32^1_0. Both of these spectra show a strong progression of ν_{39}.

From this process, the peak in the LIF spectrum is unambiguously assigned. The frequency of the ν_{39} in the excited state is lower than ground state by 10 cm^{-1} in the anti conformer, and by 11 cm^{-1} in the syn conformer. In *t*βms, the corresponding vibration (the ν_{28} according to Sinclair et al.'s numbering scheme, which did not count internal methyl vibrations[18], and the ν_{33} according to the classic Mulliken numbering scheme[1]) appears at 347 cm^{-1} in the S_0 and 283 cm^{-1} in the S_1. This difference is significantly greater than that in anethole, and suggests that in anethole this vibration changes less in the transition from the ground to the excited state in anethole than it does in *t*βms. Sinclair et al. attributed the observed decrease in the frequency of this vibration, which is the C=C-C in plane bending mode, to a decreased double bond character in the C(α)-C(β) bond[18], suggesting that this decrease is considerably less in anethole. The double bond character of this bond would likely be reduced because it "donates" some of its bonding character to the bond between C(α) and the ring. If this decrease is less, it should correspond to a smaller increase in the C(α)-C(1) bond order as well. This might in turn

cause a smaller increase in the vinyl torsional mode frequency in the S_1 state, but as we have not yet found the S_1 torsional band, this is not confirmed.

Another SVLF that exhibits this false origin behavior is that of the peak at 33019 cm^{-1} in the LIF spectrum. This peak is assigned to the 41^1_0 transition of the syn conformer, based on the frequency of the $41^1_0 63^0_2$, which appears 59 cm^{-1} below the excitation frequency, in good agreement with the 63^0_2 transition in the syn origin SVLF. This peak, and the $41^1_0 63^0_1 62^0_1$ peak are the only peaks appearing at a higher frequency than the false origin at 121 cm^{-1} below the excitation. This frequency matches the frequency of the 41^0_1 transition of the syn conformer origin SVLF. As with the previously discussed SVLF, several small peaks corresponding to the low frequency modes observed in the origin SVLF appear following this false origin. We can additionally see a transition 447 cm^{-1} below the excitation frequency, which is assigned to the $39^0_1 41^1_1$, and additional low frequency modes built off of this band. The transition at 33090 cm^{-1} in the LIF appears very similarly in the SVLF, and is assigned to the 41^1_0 transition of the anti conformer based on the frequencies of the transitions in the SVLF. These SVLFs have similar patterns but again exhibit some differences in intensity, in agreement with the differences in intensity observed in the origin SVLF. For example, the $38^0_1 41^1_1$ and $39^0_1 41^1_1$ transitions in the anti conformer SVLF have almost the same intensities. In the syn conformer SVLF, the transition involving ν_{39} is much more intense. This behavior is reflected in the origin SVLFs as well. In both of these vibrations there is very little change between the S_0 and S_1 frequencies, with a difference of only 9 cm^{-1} for the syn conformer and 7 cm^{-1} for the anti conformer. This is in good

agreement with *t*βms results, which had a difference between the S_0 and S_1 states of the corresponding ν_{34} (by the Mulliken numbering scheme) vibration of only 12 cm^{-1}.

The SVLF of the band at 33429 cm^{-1} also exhibits this behavior, and is dominated by an intense peak at 567 cm^{-1} below the excitation frequency. Based on the presence of this transition, and in comparison with calculations, this peak is assigned to the 36^1_0 transition of the syn conformer. Because the false origin is so far shifted from the excitation energy, and because the 36^1_0 band has appreciable intensity, the $36^1_039^0_1$ and the $36^1_038^0_1$ transitions are also visible at 323 cm^{-1} and 382 cm^{-1} below the excitation frequency, respectively. The frequencies of these transitions match up well with their counterparts in the origin SVLF of the syn conformer, further confirming this band as belonging to this conformer.

More complex SVLFs

In general, this strict false origin behavior in which very few transitions appear at higher frequencies than the false origin transition is an indication that there is little Duschinsky mixing of this mode in the excited state. The band at 33544 cm^{-1}, which is assigned to the 35^1_0 transition of the anti conformer, is an example of a spectrum that, while still fairly easily assigned, clearly exhibits some mixing that leads to behavior other than that discussed previously.

In this spectrum, there is appreciable activity in the region with frequency right above the most intense band. The band 578 cm^{-1} below the excitation energy is assigned to the $35^1_036^0_1$ transition, and has an intensity that is actually greater than the transition at the laser resonance. If no mixing was occurring, one would expect to see an intensity

pattern consistent with the one observed in the origin SVLF of that conformer, scaled to the size of the resonance peak, until the false origin peak was reached, at which point a new origin-like pattern would be built off that transition. This result suggests that some mixing is occurring that confers greater intensity on this transition than it has in the origin SVLF.

A similar effect is observed in the spectrum of the band at 33351, assigned as the 38^1_0 transition of the anti conformer, based on the presence of the 63^0_2 vibration combined with several different modes at an interval of 64 cm^{-1} from those modes it was built off of. 2 strong bands are observed close to one another, one at 378 and one at 408 cm^{-1} below the excitation frequency. Feasibly, either one of these could be the peak corresponding to the vibration in the excited state with which we are concerned. The peak shifter further from the excitation frequency corresponds well to the calculated frequency of ν_{38} for the anti conformer in the S_0 state. The peak at 378 cm^{-1} below the excitation corresponds well to the combination of one quantum of ν_{39} and two quanta of ν_{63} in S_0. However, it is unlikely that the excitation corresponds to this peak. Based on another assignment, the excited state frequency of ν_{39} is already known. If the excitation at anti 0^0_0 + 392 cm^{-1} corresponded to this combination, this would make the frequency of ν_{63} in S_1 only 43 cm^{-1}. Comparison with literature on similar molecules suggests that in the excited state the vinyl torsional mode should appear at a considerably higher frequency in the excited state than in the ground[9,18]. In *t*βms, for example, the torsional mode appears at 28 cm^{-1} in S_0 and 165 cm^{-1} in S_1. It therefore seems unlikely that this is the correct assignment, and we instead assign this spectrum as arising from the 38^1_0 transition, the stronger of the two intense bands to the 38^1_1 and the weaker of the two

strong bands to the $38^1_0 39^1_0 63^0_2$. Again, based on what has been seen in the origin SVLF, one would expect the $39^1_0 38^0_1 63^0_2$ would have less intensity than the $39^1_0 38^0_1$. The observed greater intensity suggests that the Duschinsky effect is at work.

Several SVLF spectra have been collected that are even more complex than these. These spectra typically arise from combination bands or overtones. 2 examples of these bands are the syn and anti 61^2_0 bands, at 33065 cm^{-1} and 33122 cm^{-1}, respectively, which correspond to relative wavenumbers of 177 cm^{-1} and 163 cm^{-1}. These bands are assigned mostly through trial and error: we look for relatively strong peaks in the SVLF and try to match them to combinations of the vibrations in the ground state. In this case, there is a strong band in the anti conformer at 214 cm^{-1}, in good agreement with two quanta of the ν_{61} in the ground state. This peak was the most intense peak in the anti SVLF spectrum, but in the syn, the corresponding peak at 222 cm^{-1} was not most intense, but rather the peak at 181 cm^{-1} below the excitation frequency dominated the spectrum. This made the syn conformer spectrum more difficult to assign, and it was only after the anti spectrum was assigned that similarities were identified and the corresponding peak in the LIF was identified. The anti conformer is therefore more completely assigned. This spectrum appears much more complex because of the coupling of the ν_{61} with a variety of other modes including the 63, 41, and 39 vibrations. These combinations allow us to observe some odd quanta of out of plane motions, since they are in combination with each other. A similar mode does not appear in either *t*βms or anisole, making literature comparison of little value in confirming this assignment.

As more mixing and more combination bands come into play, it becomes more difficult to reliably assign spectra to specific transitions. For this reason, some SVLF

spectra are assigned only to one conformer, but not to a specific transitions. It is expected that with more time, one could identify a few possibilities for each corresponding transition in the LIF based on the combination bands visible in these SVLFs.

Water SVLF Spectra

For several of the SVLF spectra in the low frequency region, anomalous behavior was observed. In most SVLFs the transition closest to the excitation frequency is the 63^0_2, which never appears below 50 cm^{-1}. However, in the SVLF of the band at 32977 cm^{-1}, we see additional bands at 23 and 41 cm^{-1} below the excitation wavelength. Similarly, for the SVLF of the band at 33029 cm^{-1} and 32977 cm^{-1}, bands below 50 cm^{-1} are also visible. This suggests that these bands arise from something other than neat anethole. We hypothesize that these bands come from excitation of anethole-water Van der Waals complexes. Seeding water into the gas line and taking an LIF of the low wavenumber region confirms this hypothesis, as we see bands grow in that correspond to the SVLF excitations of these 4 bands. Due to limited information about the nature of these clusters and their shapes, we have yet to assign them to specific vibrations or cluster formations. However, we do still see the diagnostic 63^0_2 and 39^0_1 vibrations, suggesting that these modes are relatively unchanged by the addition of the water molecule. This is not surprising, since previous work[30, 34,32,] suggests that the water molecule interacts with the methoxy and the ring, but most likely not with the vinyl group. The 63 and 39 vibrations are mostly based on the vinyl group, and therefore should see little perturbation when water is added.

Potential Energy Scans

Potential energy scans of the anethole vinyl torsion, shown in Figure (PE scans) show an anharmonic potential energy surface. MP2 calculations predict that at the bottom of each large well are two smaller wells, corresponding to energy minima when the vinyl group is slightly out of plane. HF calculations also predict this, while DFT calculations show that the minimum is at the point where the vinyl group is coplanar with the ring. Based on what we have seen in the spectra, we know that anethole has a heavy atom planar structure. Therefore, we take the DFT calculations to be the most accurate in predicting the geometry at which the minimum occurs. However, this does not necessarily mean that the parameters of the Fourier transform fit (equation 1) calculated from the DFT data are the most accurate. Based on comparison with the literature, MP2 calculations give the best approximation of the barrier to isomerization through the vinyl torsion, of 873.67 cm^{-1}.

We can get an even better sense of the proximity of our calculation of the barrier to isomerization to actual values by comparing the values we calculated for the *t*βms torsion with those simulated by Sinclair et al.[18] using experimental information. Our calculations predict this barrier to be 817 cm^{-1}. Fitting experimental data, Sinclair et al. calculate the barrier to isomerization through the vinyl torsion to be 855 cm^{-1}. Liu et al.[9] provide a comparison between calculations at the MP2/6-31+G(d,p) level and their simulation from experimental values for this barrier as well. The barrier to the vinyl rotation in (E)-PVA from calculations is found to be 846 cm^{-1}, and from fitting the experimental data is found to be 688 cm^{-1}. While this calculation still significantly

overestimates the barrier, it is the most accurate of the calculations they tried, including HF/6-311++g(d,p), which gave a barrier of 1095 cm^{-1}, and B3LYP/6-311g++(d,p), which gave a barrier of 1674 cm^{-1}. Furthermore, we used a larger basis set for our MP2 calculations, suggesting that our calculated values should be even closer to experimental. It seems reasonable to take the value of the barrier to the vinyl isomerization obtained from our MP2 calculations as a fairly good estimate of the actual barrier.

Determining the accuracy of the anharmonicity term from the calculation is a bit more difficult. Based on data from Liu et al.[9], HF calculations actually predict this term best. For (E)-PVA, HF calculations gave a V_4 term of -297 cm^{-1}, while the value from experimental data is -114 cm^{-1}. Again, this is still quite a large overestimate but all other calculations overestimate this value even further. Our calculation of the *t*βms vinyl torsional barrier at the HF level of theory gives a value of -204 cm^{-1}, and is the closest to the experimental value of -218 cm^{-1}. We therefore take the HF calculation as the most accurate estimate of the barrier to the vinyl rotation in anethole.

Based on our calculations, the vinyl rotation of anethole and *t*βms have very similar barriers, different by only about 57 cm^{-1} based on calculations.. This is to be expected: the torsional vibrations of anethole and *t*βms appear only a few cm^{-1} different in frequency. Furthermore, we have seen in the spectroscopy that in the ground state the vinyl group can move independently of the methoxy group (based on repeated presence of the 63^0_2 transition). This would suggest that the addition of the methoxy should have very little effect on the torsional motion of the vinyl group.

We have also performed the same scan for the methoxy rotation of anethole, and, for comparison, of anisole. It is difficult to say how accurate these scans are since the literature on anisole does not generally calculate the barrier to this rotation, likely because they did not observe a purely torsional mode of anisole. In general, the methoxy rotations of both molecules exhibit the reverse from the vinyl torsion anharmonicity, with a narrowing of the potential rather than a flat bottom, corresponding to a positive V_4 term. There is no evidence in the spectrum of the methyl torsions, so these modes were not modeled.

Comparison with Similar Systems

Anethole exhibits several features that are quite similar to other styrene derivatives, and to anisole, particularly its benzene-like modes. A comparison of some of these modes is shown in Table 12. Anethole, at least with respect to these two modes, which were the only two benzene-like modes assigned for both conformers, seems to be more different from the other substituted benzenes than these molecules are from each other, with the exception of anisole. This suggests that in order for closely matching frequencies to be observed, it is not enough to simply be a substituted benzene, the molecule must be of a similar class. Both of these ring modes must be at least somewhat substituent sensitive in order to be affected by the addition of the methoxy.

Table 12. comparison of some benzene like vibrations between anethole and similar molecules.

	v1		v6b	
molecule	s0	s1	s1	s1
syn-anethole	849		651	585
anti-anethole	847		644	
*t*βms[18]	621	537	821	795
styrene[19]	624	528	776	746
(E)-PVA[9]	623	539	851	815
anisole[26]	782	758	616	499

The ν_{63} and ν_{39}

transitions also have counterparts in styrene and in *t*βms. Comparisons between the frequencies of these modes in anethole and in *t*βms and styrene therefore can provide some useful information. For example, the 63^0_2 vibration of anethole appear at a very similar frequency to the same vibration in *t*βms at 67 cm^{-1}. However, styrene exhibits a similar mode much higher in energy, at 85 cm^{-1}. This change likely is a result of the addition of the methyl group to the vinyl. This makes the rotor heavier, and leading to a lower frequency vibration. However, the close proximity to the value for *t*βms suggests that the methoxy group plays a very small role in this vibration.

In contrast, the 39^0_1 vibration is effected by the presence of the methoxy group. In *t*βms, this vibration appears at 385 cm^{-1}, while in anethole it appears at 325 cm^{-1} and 317 cm^{-1}. In styrene, a comparable vibration appears at 395 cm^{-1}. The close proximity of the frequencies for *t*βms and styrene suggest that the methyl group is likely not what is causing this perturbation. The only other culprit would be the methoxy substituent. This should not be too surprising since, unlike the 63 vibration, which showed mainly a motion of the vinyl torsional mode, the 39 vibration involves in-plane bending of both substituent groups.

Comparison with anisole has, for the most part, been conspicuously absent. This is due to the fact that the spectrum of anethole is dominated by benzene-like modes and modes that are very similar to those of *t*βms. In fact, examination of the calculated normal modes reveals that there is no mode in which the rotation of the methoxy group is the only motion, while there is at least one mode (the 63 vibration) that depends almost exclusively on the vinyl group. This allows some of the motions of the vinyl group to remain essentially unchanged by the addition of the methoxy, but means that torsions that

involve the methoxy mode will be changed by the vinyl substituent, making the vibrational structure of anethole look much more like that of *t*βms.

Future Work

Much of the LIF spectrum, and many of the SVLFs remain unassigned. Even more time could be spent puzzling these spectra together. Furthermore, because we are unsure exactly where the vinyl torsional mode should appear in the LIF, if more bands were assigned, we might be able to identify this mode by process of elimination.

We have observed a progression of the torsional mode in the S_0 state, and from this data it should be feasible to complete a simulation of the torsional potential in the S_1 state to be compared with calculation results.

A rich area for further work is in the investigation of water clusters, which we are now fairly certain anethole forms[30,34,31]. Water could feasibly interact with either the pi cloud of the ring system or the oxygen. Further studies, and high level calculations of the cluster structures would be necessary to determine exactly how the water and anethole molecules are interacting and to assign the SVLF bands of the water-anethole clusters.

Further work could also focus on an investigation of the cis isomer of anethole. Anethole has been shown to exhibit photoisomerization[3], and the *cis*-isomer should therefore be relatively simple to produce. Thus far, we have compared anethole only to nonsterically hindered styrene derivatives, but the *cis* isomer would likely exhibit some steric clash between the methyl group on the vinyl and the ring hydrogens. This would potentially cause *cis*-anethole to be nonplanar, giving a very different spectrum than *trans*-anethole, as the planarity selection rule would no longer apply.

Conclusion

In this work, the Jet-Cooled UV spectroscopy of anethole was undertaken, in order to gain information about the vibrational modes in the S_0 and S_1 states. The LIF spectrum of *trans*-anethole is presented and partially assigned. Anethole was found to be planar, and to have two conformers. The barrier of isomerization between these two conformers, and the anharmonicity of the potential for the transformation from one conformer to the other via both possible coordinates of isomerizaton were determined using *ab initio* calculations. Several SVLF spectra of bands in the LIF are also reported and assigned, primarily those due to first overtones of in-plane bending modes. SVLFs of combination bands and overtones prove much more complicated and few of these SVLFs have been assigned to specific transitions. In most cases, however, we were able to observe a few diagnostic transitions in order to at least assign a transition to the *syn* or *anti* conformer. It was found that anethole exhibits several benzene like modes, and additionally has some similar spectroscopic features to *t*βms, but has very little in common with anisole. We also observed some features in experimental data that could be attributed to Van der Waals clusters between anethole and water. Opportunities for further work include the further study of these water clusters, the completion of the assignments of bands in the LIF and some of the SVLFs, the modeling of the torsional potential based on experimental data, and the investigation of *cis*-anethole.

Works Cited

1. MULLIKEN, R., *Journal of Chemical Physics* **1955,** *23* (10), 1833-1840.
2. *Test Plan for Anethole (isomer unspecefied) and trans-anethole*; The Flavor and Fragrance High Production Volume Consortia: Washington, DC, 2002.
3. Castro, H.; Martinez, J.; Stashenko, E., *Molecules* **2010,** *15* (7), 5012-5030.
4. NOZAKI, H.; OTANI, I.; NOYORI, R.; KAWANISI, M., *Tetrahedron* **1968,** *24* (5), 2183-&.
5. GRASSIAN, V.; BERNSTEIN, E.; SECOR, H.; SEEMAN, J., *Journal of Physical Chemistry* **1989,** *93* (9), 3470-3474.
6. LEVY, D., *Annual Review of Physical Chemistry* **1980,** *31*, 197-225.
7. VAIDA, V., *Accounts of Chemical Research* **1986,** *19* (4), 114-120.
8. ITO, M.; EBATA, T.; MIKAMI, N., *Annual Review of Physical Chemistry* **1988,** *39*, 123-147.
9. Liu, C.; Newby, J.; Muller, C.; Lee, H.; Zwier, T., *Journal of Physical Chemistry a* **2008,** *112* (39), 9454-9466.
10. BECKE, A., *Journal of Chemical Physics* **1993,** *98* (2), 1372-1377.
11. LEE, C.; YANG, W.; PARR, R., *Physical Review B* **1988,** *37* (2), 785-789.
12. MCLEAN, A.; CHANDLER, G., *Journal of Chemical Physics* **1980,** *72* (10), 5639-5648.
13. FRISCH, M.; POPLE, J.; BINKLEY, J., *Journal of Chemical Physics* **1984,** *80* (7), 3265-3269.
14. Herzberg, G., *Molecular Spectra and Molecular Structure*. Van Nostrand-Reinhold: New York, 1996; Vol. III.
15. Wilson, E. B., *Phys. Rev.* **1934,** *45*.
16. Duschinsky, F., *Acta Phisicochim. URSS* **1937,** *7*, 551-566.
17. FORESMAN, J.; HEADGORDON, M.; POPLE, J.; FRISCH, M., *Journal of Physical Chemistry* **1992,** *96* (1), 135-149.
18. Sinclair, W. E.; Yu, H.; Phillips, D.; Gordon, R. D.; Hollas, J. M.; Klee, S.; Mellau, G., *J. Phys Chem* **1995,** *99* (13), 4386-4396.
19. HOLLAS, J.; RIDLEY, T., *Chemical Physics Letters* **1980,** *75* (1), 94-98.
20. Moller, C.; Plesset, M., *Physical Review* **1934,** *46* (7), 0618-0622.
21. FRISCH, M.; HEADGORDON, M.; POPLE, J., *Chemical Physics Letters* **1990,** *166* (3), 281-289.
22. ROOTHAAN, C., *Reviews of Modern Physics* **1951,** *23* (2), 69-89.
23. MCWEENY, R.; DIERCKSEN, G., *Journal of Chemical Physics* **1968,** *49* (11), 4852-&.
24. HOLLAS, J.; KHALILIPOUR, E.; THAKUR, S., *Journal of Molecular Spectroscopy* **1978,** *73* (2), 240-265.
25. DURIG, J.; GUIRGIS, G.; BELL, S., *Journal of Physical Chemistry* **1989,** *93* (9), 3487-3491.
26. Matsumoto, R.; Sakeda, K.; Matsushita, Y.; Suzuki, T.; Ichimura, T., *Journal of Molecular Structure* **2005,** *735*, 153-167.
27. Ribeiro-Claro, P. J. A.; Teixeira-Dias, J. J. C.; Hollas, J. M.; Milewski, M., *J. Chem. Soc. Faraday Trans.* **1995,** *91* (2), 197-203.
28. HOLLAS, J.; TADAY, P.; GORDON, R., *Journal of Molecular Spectroscopy* **1992,** *153* (1-2), 587-598.
29. HOLLAS, J.; BINHUSSEIN, M., *Journal of Molecular Spectroscopy* **1991,** *145* (1), 89-99.
30. Becucci, M.; Pietraperzia, G.; Pasquini, M.; Piani, G.; Zoppi, A.; Chelli, R.; Castellucci, E.; Demtroeder, W., *Journal of Chemical Physics* **2004,** *120* (12), 5601-5607.
31. PRIBBLE, R.; ZWIER, T., *Faraday Discussions* **1994,** *97*, 229-241.
32. Gruenloh, C.; Carney, J.; Arrington, C.; Zwier, T.; Fredericks, S.; Jordan, K., *Science* **1997,** *276* (5319), 1678-1681.

33. Pribble, R.; Hagemeister, F.; Zwier, T., *Journal of Chemical Physics* **1997,** *106* (6), 2145-2157.
34. Barth, H.; Buchhold, K.; Djafari, S.; Reimann, B.; Lommatzsch, U.; Brutschy, B., *Chemical Physics* **1998,** *239* (1-3), 49-64.
35. Physical Constants of Organic Compounds. In *CRC Handbook of Chemistry and Physics*, 93rd ed.; Lide, D. R., Ed. 2013; p 352.
36. Pillsbury, N.; Muller, C.; Zwier, T., *Journal of Physical Chemistry a* **2009,** *113* (17), 5013-5021.
37. Newby, J.; Liu, C.; Muller, C.; James, W.; Buchanan, E.; Lee, H.; Zwier, T., *Journal of Physical Chemistry a* **2010,** *114* (9), 3190-3198.
38. de Groot, M.; Buma, W.; Gromov, E.; Burghardt, I.; Koppel, H.; Cederbaum, L., *Journal of Chemical Physics* **2006,** *125* (20).
39. Bauernschmitt, R.; Ahlrichs, R., *Chemical Physics Letters* **1996,** *256* (4-5), 454-464.
40. Scalmani, G.; Frisch, M.; Mennucci, B.; Tomasi, J.; Cammi, R.; Barone, V., *Journal of Chemical Physics* **2006,** *124* (9).
41. Frisch, M. J.; Trucks, G. W.; Schlegel, H. B.; Scuseria, G. E.; Robb, M. A.; Cheeseman, J. R.; Scalmani, G.; Barone, V.; Mennucci, B.; Petersson, G. A.; Nakatsuji, H.; Caricato, M.; Li, X.; Hratchian, H. P.; Izmaylov, A. F.; Bloino, J.; Zheng, G.; Sonnenberg, J. L.; Hada, M.; Ehara, M.; Toyota, K.; Fukuda, R.; Hasegawa, J.; Ishida, M.; Nakajima, T.; Honda, Y.; Kitao, O.; Nakai, H.; Vreven, T.; Montgomery, J., J. A.; Peralta, J. E.; Ogliaro, F.; Bearpark, M.; Heyd, J. J.; Brothers, E.; Kudin, K. N.; Staroverov, V. N.; Kobayashi, R.; Normand, J.; Raghavachari, K.; Rendell, A.; Burant, J. C.; Iyengar, S. S.; Tomasi, J.; Cossi, M.; Rega, N.; Millam, J. M.; Klene, M.; Knox, J. E.; Cross, J. B.; Bakken, V.; Adamo, C.; Jaramillo, J.; Gomperts, R.; Stratmann, R. E.; Yazyev, O.; Austin, A. J.; Cammi, R.; Pomelli, C.; Ochterski, J. W.; Martin, R. L.; Morokuma, K.; Zakrzewski, V. G.; Voth, G. A.; Salvador, P.; Dannenberg, J. J.; Dapprich, S.; Daniels, A. D.; Farkas, O.; Foresman, J. B.; Ortiz, J. V.; Cioslowski, J.; Fox, D. J. *Gaussian 09*, Gaussian, Inc., : Wallingford, CT, 2009.
42. Dooley, R.; Allen, G.; Pamidighantam, S. In *Computational Chemistry Grid: Production Cyberinfrastructure for Computational Chemistry*, The 13th Annual Mardi Gras Conference, Baton Rouge, LA, Baton Rouge, LA, 2005.
43. Milfield, K.; Guiang, C.; Pamidighantam, S. In *Computing through an Application Oriented Computational Chemistry Grid*, 2005 Linux Clusters: The HPC Revolution, 2005.
44. Haas, Y.; Kendler, S.; Zingher, E.; Zuckermann, H.; Zilberg, S., *J. Phys. Chem.* **1995,** *103* (1), 37-46.
45. ONDA, M.; TODA, A.; MORI, S.; YAMAGUCHI, I., *Journal of Molecular Structure* **1986,** *144* (1-2), 47-51.
46. HOLLAS, J.; MUSA, H.; RIDLEY, T.; TURNER, P.; WEISENBERGER, K.; FAWCETT, V., *Journal of Molecular Spectroscopy* **1982,** *94* (2), 437-455.
47. Hehre, W., Computational Chemistry. 2010.